

Drought response of the boreal forest carbon sink is driven by understorey–tree composition

Received: 28 October 2022

Accepted: 8 January 2024

Published online: 13 February 2024

 Check for updates

Eduardo Martínez-García ^{1,2}✉, Mats B. Nilsson ¹, Hjalmar Laudon ¹,
Tomas Lundmark¹, Johan E. S. Fransson ^{3,4}, Jörgen Wallerman ³ &
Matthias Peichl ¹

The boreal forest is an important global carbon sink, but its response to drought remains uncertain. Here, we compiled biometric- and chamber-based flux data from 50 boreal forest stands to assess the impact of the 2018 European summer drought on net ecosystem production (NEP) across a 68 km² managed landscape in northern Sweden. Our results reveal a non-uniform reduction in NEP (on average by 80 ± 16 g C m⁻² yr⁻¹ or $57 \pm 13\%$) across the landscape, which was greatest in young stands of 20–50 years (95 ± 39 g C m⁻² yr⁻¹), but gradually decreased towards older stands (54 ± 57 g C m⁻² yr⁻¹). This pattern was attributed to the higher sensitivity of forest-floor understorey to drought and its decreasing contribution to production relative to trees during stand development. This suggests that an age-dependent shift in understorey–tree composition with increasing stand age drives the drought response of the boreal forest NEP. Thus, our study advocates the need for partitioning ecosystem responses to improve empirical and modelling assessments of carbon cycle–climate feedbacks in boreal forests. It further implies that the forest age structure may strongly determine the carbon sink response to the projected increase in drought events across the managed boreal landscape.

Boreal forests cover 11% of the Earth's land surface¹ and store around one-third of the global terrestrial carbon (C) stock². As such, they are recognized as an important element in climate change mitigation policies³. Yet, the circumpolar boreal region is subject to the fastest rate of climatic change^{4,5}. This includes more frequent and severe extreme climatic events such as droughts^{6,7}, which are expected to diminish the C sink strength of this biome during the twenty-first century⁸. Advancing our understanding of how the forest C cycle responds to droughts is hence crucial for improving the predictions of boreal forest C cycle–climate feedback.

Drought stress in forest ecosystems commonly arises from prolonged periods of reduced precipitation combined with warm air temperature, causing high evaporative demand coupled with decreasing soil water availability⁹. The impact of drought on the forest net ecosystem production (NEP; that is, the ecosystem C balance) therefore depends on the distinct responses of its two primary underlying components, that is, net primary production (NPP) and heterotrophic respiration (RH), to both warmer and drier conditions. In situ experiments¹⁰, remote sensing^{11,12} and ecological modelling¹³ studies suggest that droughts reduce forest NPP primarily through suppression of photosynthetic activity by

¹Department of Forest Ecology and Management, Swedish University of Agricultural Sciences, Umeå, Sweden. ²Natural Resources Institute Finland (Luke), Helsinki, Finland. ³Department of Forest Resource Management, Swedish University of Agricultural Sciences, Umeå, Sweden. ⁴Department of Forestry and Wood Technology, Linnaeus University, Växjö, Sweden. ✉e-mail: eduardo.martinez@slu.se; eduardo.martinezgarcia@luke.fi; edu.martinez.garcia@gmail.com

either ecophysiological or structural changes in plants, plant hydraulic damage, and/or forest dieback through concurrent abiotic and biotic stress^{14,15}. At the same time, the increase in temperature occurring during droughts may stimulate RH rates¹⁶. However, beyond a certain threshold, RH might also become constrained if drought conditions lead to soil water stress on microbial communities¹⁷. Despite this understanding from previous works, considerable uncertainty remains about the relative importance of these processes in mediating the drought response of the forest NEP across the boreal landscape.

The variation in the drought-induced reduction in forest NPP is often attributed to differences in tree age and/or size^{18–23}. Nonetheless, while most of this knowledge has been developed in temperate and tropical regions, empirical evidence supporting this dependency remains limited for boreal forests. Furthermore, most previous studies ascribe the impact of drought on NPP to the response of the tree layer, while less attention has been paid to that of the understorey vegetation. However, relative to deep-rooted trees, the understorey vegetation growing on the forest floor has been reported to be particularly vulnerable to drought stress because of shallower rooting depths and smaller C reserves^{24,25}. Given that the understorey may contribute up to 80% to NPP in the boreal forest²⁶, there is a critical need to account for the role of this component in both empirical and modelling assessments of drought impacts on the boreal forest C sink.

Most recently, several studies using eddy covariance measurements have provided valuable evidence regarding the impact of drought on the boreal forest NEP^{9,27–30}. Nevertheless, eddy covariance studies provide limited insights into how the response of NEP to drought is regulated by the sensitivity of its underlying production and respiration component fluxes. In addition, eddy covariance studies commonly suffer from a lack of spatial replication, therefore failing to capture the large heterogeneity across the boreal landscape. In comparison, networks of extensively distributed and repeatedly measured monitoring plots that use biometric- and chamber-based measurements may provide valuable information on the variability in the drought response of the separate forest NEP component fluxes across the heterogeneous landscape.

During the summer of 2018, a record-breaking, hot drought occurred over extensive regions of Central and Northern Europe³¹. This study explored its consequences for the boreal forest C balance across a 68 km² managed boreal landscape located in northern Sweden (Extended Data Fig. 1). Compared with the nearly normal environmental conditions observed in this landscape during the baseline period 2016–2017, the year 2018 was characterized by an exceptionally warm and sunny, but normally wet spring. It was followed by an unusual summer marked by moderate drought conditions in May and June, which reached severe levels in July (Fig. 1). The progression of the summer drought was primarily caused by extremely high positive anomalies in air temperature and radiation rather than by precipitation deficits. The environmental conditions at the forest-floor interface further confirmed that temperature rather than moisture was the main driver of the summer drought development (Supplementary Fig. 1). To investigate the landscape-scale variation in the response of forest NEP and its component fluxes to this exceptional 2018 drought relative to the baseline period 2016–2017, we used an extensive dataset of biometric- and chamber-based annual CO₂ flux measurements obtained in 50 forest stands (spanning 5 to 211 years old) located across the landscape. Specifically, we analysed the distinct drought responses of forest-floor understorey and tree NPP as well as RH to understand how these in concert regulate the magnitude of the drought impact on the forest ecosystem C balance.

Non-uniform drought response of NEP across the forest landscape

During the drought year 2018, NEP decreased on average by 80 ± 16 g C m⁻² yr⁻¹ (mean \pm 95%CI; Fig. 2a,b), which corresponds to a reduction of

$57 \pm 13\%$ (Extended Data Fig. 2a) across the studied landscape. Nevertheless, our findings reveal a non-uniform response across stand ages. Specifically, a twofold greater NEP reduction was observed in 20–50 year old stands, averaging at 95 ± 39 g C m⁻² yr⁻¹, compared with a reduction of 54 ± 57 g C m⁻² yr⁻¹ in stands older than 130 years (Fig. 2b). It is further noteworthy that the drought induced a transition from C sink to source in only a small number of forest stands, mainly in young and low productive mature ones (Fig. 2a). Our results also suggest that the response of NPP rather than that of RH modulated this stand-age-related divergence in the drought impact on NEP. In particular, NPP exhibited an average decrease of 51 ± 16 g C m⁻² yr⁻¹ (Fig. 2c,d) or $13 \pm 4\%$ (Extended Data Fig. 2b), following an age-related response pattern similar to that of NEP. In comparison, RH increased on average by 29 ± 4 g C m⁻² yr⁻¹ (Fig. 2e,f) or $14 \pm 2\%$ (Extended Data Fig. 2c), but without a clear age-dependent pattern. We further noted that neither soil type nor tree species significantly affected the drought response of NEP, NPP and RH across the landscape (Extended Data Fig. 3).

The partitioning of NPP into its components (Fig. 3) showed a greater decrease in understorey production (NPP_u) compared with tree production (NPP_t), with an average reduction of 33 ± 8 and 17 ± 2 g C m⁻² yr⁻¹, respectively (or $26 \pm 5\%$ and $7 \pm 5\%$, respectively; Extended Data Fig. 4). Our results further reveal that the drought response of NEP corresponded most closely to the NPP_u anomaly in the younger forest stands up to the age of ~70 years, beyond which the NPP_t anomaly largely explained the NEP reduction (Fig. 4 and Supplementary Table 1). The shift in the relative importance of NPP_u to NPP_t in regulating the response of NEP to drought coincided with a decrease in their ratio with stand age (Fig. 5). Specifically, NPP_u was the dominant contributor to NPP in young forest stands (≤ 25 years), whereas NPP_t became the more important component of NPP in older stands. Consequently, the age-related reduction in NEP (Fig. 2a,b) was the result of the greater drought sensitivity of understorey and its decreasing contribution to NPP relative to trees as stands aged. We also found that drought reduced aboveground production rather than belowground production in trees (Extended Data Fig. 5), whereas for understorey vegetation, both above- and belowground production were vulnerable to drought (Extended Data Fig. 6). In addition, no effect of soil type and tree species was observed on the drought response of NPP_t and NPP_u (Extended Data Fig. 7).

We further analysed a greenness index (that is, green chromatic coordinate, gcc) to describe the seasonal phenology of understorey (gcc_u) and trees (gcc_t) in a mature mixed-species forest stand located within the studied landscape (Methods and Extended Data Fig. 1). During the 2018 growing season, gcc_u decreased by 36%, which was threefold greater than the decrease in gcc_t (12%; Fig. 6). In addition, the timing and length of the peak growing season were affected differently for trees and understorey during the drought year, with larger changes observed in the latter component.

Understorey–tree composition controls drought impact on NEP

Our empirical evidence for the shift in understorey–tree composition with increasing stand age as a key control adds an improved conceptual dimension for evaluating the landscape-scale sensitivity of the forest C balance to drought. This result suggests that the common exclusive focus on the tree layer may lead to considerable bias in estimating the drought response of the boreal forest C sink. Consequently, there is a need to alleviate the widespread deficiency in understorey sampling³² in future biometric-based studies, particularly in young boreal forest stands where understorey exerts a key control on regulating the drought-induced NEP change. Furthermore, the different responses of forest-floor understorey and tree NPP to drought, and how they in concert regulate the drought sensitivity of NEP, call for further efforts to partition ecosystem responses in order to improve model-based predictions of C cycle–climate feedbacks in boreal forests.

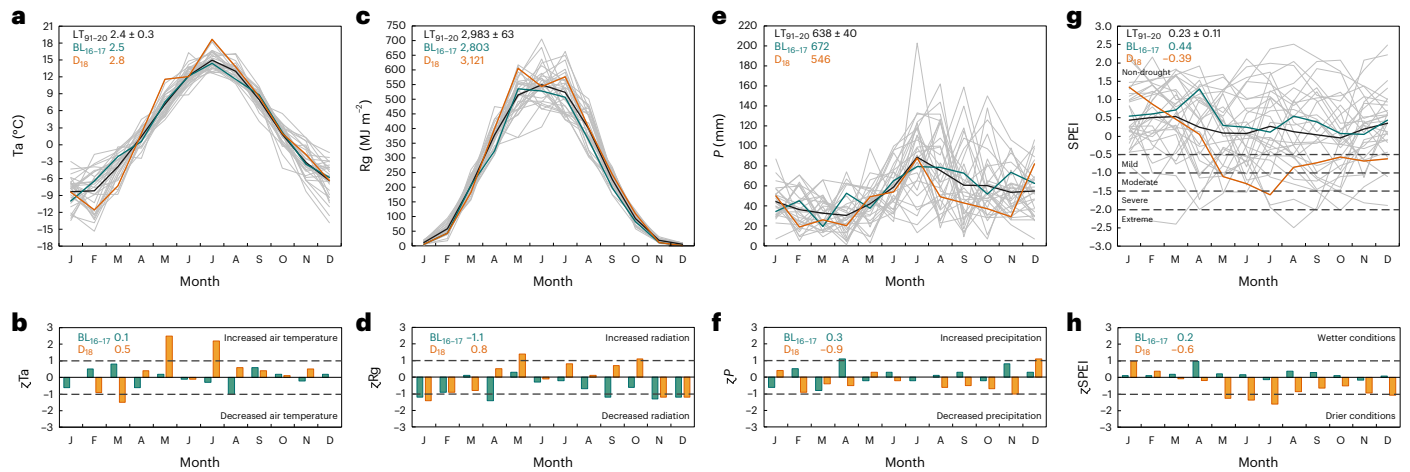


Fig. 1 | Environmental conditions during drought and reference periods. **a–h**, Air temperature (T_a , °C; **a,b**), global radiation (R_g , MJ m^{-2} ; **c,d**), precipitation (P , mm; **e,f**) and standardized precipitation evapotranspiration index at a three-month time scale (SPEI, dimensionless; **g,h**) observed during the long-term reference period 1991–2020 (LT_{91-20}), baseline period 2016–2017 (BL_{16-17}) and drought year 2018 (D_{18}). The letters on the x axes represent the first letter of each month. Drought magnitude in **g** was classified into five types including extreme ($\text{SPEI} \leq -2.0$), severe ($-2.0 < \text{SPEI} \leq -1.5$), moderate ($-1.5 < \text{SPEI} \leq -1.0$), mild

($-1.0 < \text{SPEI} \leq -0.5$) and non-drought ($\text{SPEI} > -0.5$). Values in **a**, **c**, **e** and **g** show annual means ($\pm 95\%$ confidence intervals), while the solid lines show the mean monthly values. Panels **b**, **d**, **f** and **h** show the annual and monthly standardized anomalies ($z\chi$), with values showing the annual means and bars depicting the monthly values. Extreme environmental and drought conditions are defined as values of $z\chi$ above and below one standard deviation unit, respectively (depicted as dashed lines).

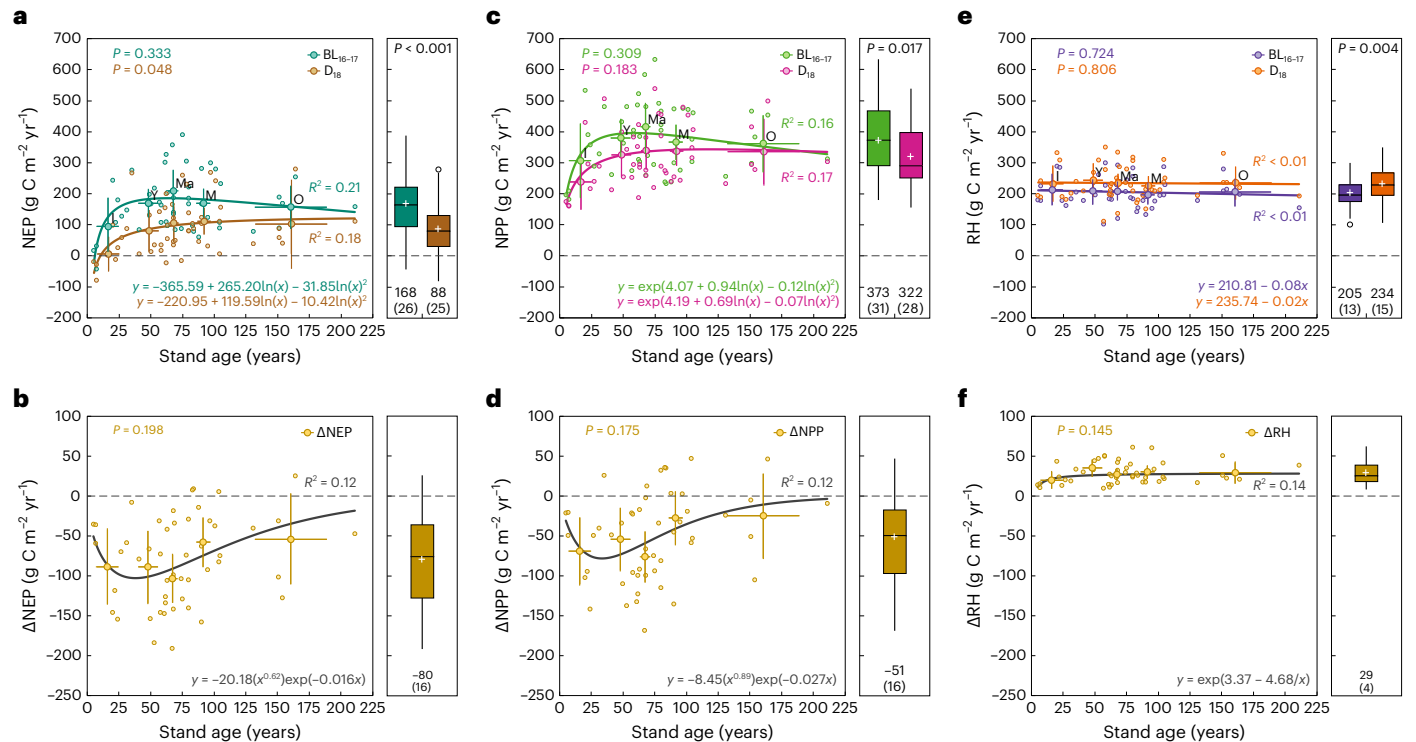


Fig. 2 | Drought response of forest NEP and its component fluxes. **a,c,e**, Annual values of NEP (**a**), NPP (**c**) and total RH (**e**) for the baseline period 2016–2017 (BL_{16-17}) and the drought year 2018 (D_{18}). **b,d,f**, Absolute anomalies (ΔX) of NEP (**b**), NPP (**d**) and total RH (**f**) (ΔX). Circular open symbols indicate the values for each forest stand, while circular filled symbols indicate the means for each of the stand age classes, including initiation (I), young (Y), middle-aged (Ma), mature (M) and old-growth (O). The horizontal and vertical bars represent the 95% confidence intervals, while the solid lines show the best-fit regressions. The equation form and coefficient of determination (R^2) of the linear regressions are also presented. Equations and associated goodness-of-fit statistics are derived

from the individual forest stand data ($n = 49$). Box plots of the annual values along with the absolute anomalies are also shown. The boxes represent the 25th (bottom) and 75th (top) percentiles, the central line the median, and the cross the mean. Whiskers above and below the boxes denote the data within 1.5 times the interquartile range, with outliers presented as individual points. The values show the means ($\pm 95\%$ confidence intervals) of NEP, NPP and RH, as well as their absolute anomalies. The P values for the non-parametric Kruskal–Wallis rank sum test comparing the differences between the means of stand age classes and BL_{16-17} – D_{18} periods are also shown. The horizontal dashed lines indicate the negative-to-positive transition for the absolute anomalies.

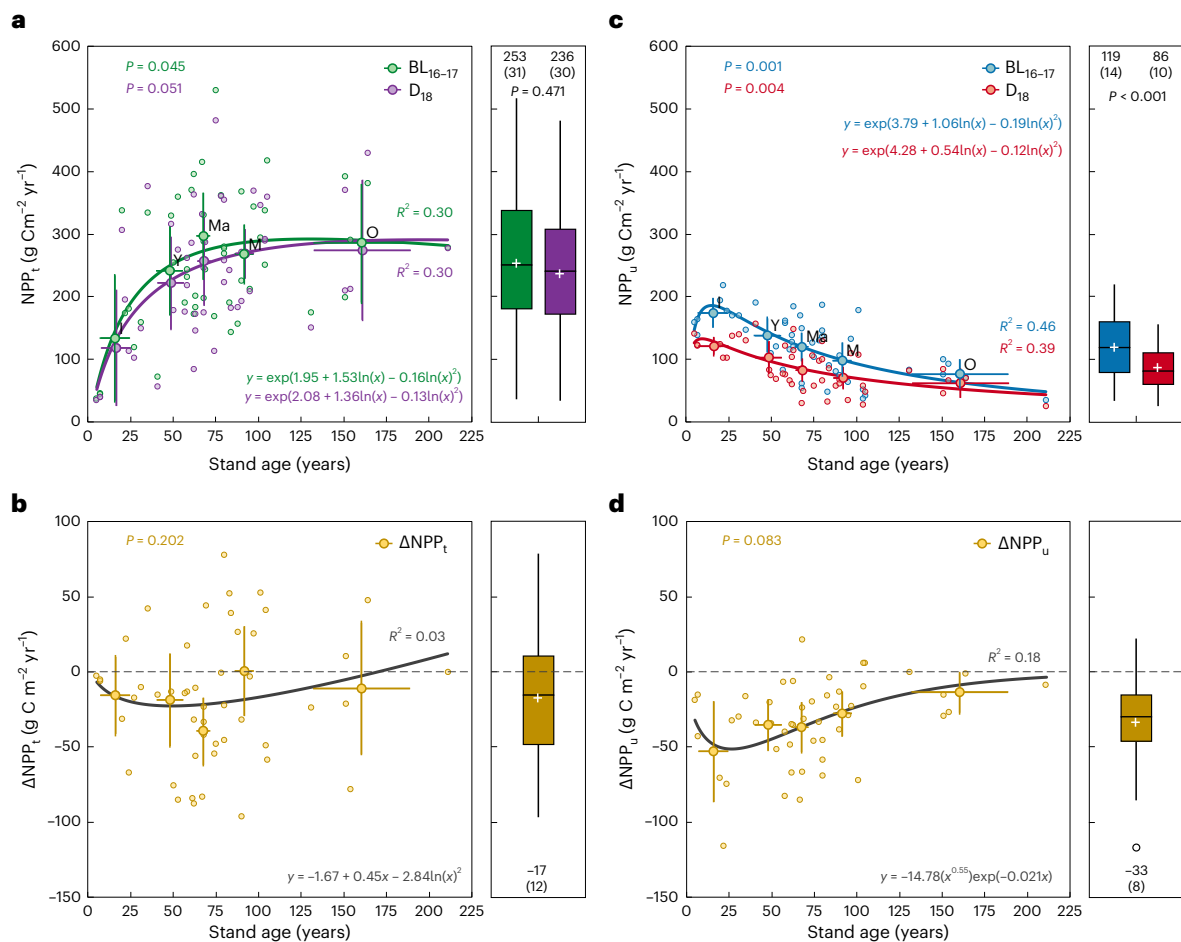


Fig. 3 | Drought response of tree and understorey NPP. a,c, Annual values of NPP of trees (NPP_t; **a**) and understorey (NPP_u; **c**) for the baseline period 2016–2017 (BL_{16–17}) and the drought year 2018 (D₁₈). **b,d,** Absolute anomalies (ΔX) of trees (ΔNPP_t ; **b**) and understorey (ΔNPP_u ; **d**) (ΔX). Circular open symbols indicate the values for each forest stand, while circular filled symbols indicate the means for each of the stand age classes, including initiation (I), young (Y), middle-aged (Ma), mature (M) and old-growth (O). The horizontal and vertical bars represent the 95% confidence intervals, while the solid lines show the best-fit regressions. The equation form and coefficient of determination (R^2) of the linear regressions are also presented. Equations and associated goodness-of-fit statistics are

derived from the individual forest stand data ($n = 49$). Box plots of the annual values along with the absolute anomalies are also shown. The boxes represent the 25th (bottom) and 75th (top) percentiles, the central line the median, and the cross the mean. Whiskers above and below the boxes denote the data within 1.5 times the interquartile range, with outliers presented as individual points. The values show the means ($\pm 95\%$ confidence intervals) of NPP_t and NPP_u, as well as their absolute anomalies. The P values for the non-parametric Kruskal–Wallis rank sum test comparing the differences between the means of stand age classes and BL_{16–17}–D₁₈ periods are also shown. The horizontal dashed lines indicate the negative-to-positive transition for the absolute anomalies.

The greater decline in understorey production compared with that of trees might reflect the lower competitiveness of shallow-rooted understorey versus deep-rooted trees during periods with soil water scarcity^{24,25}. Specifically, the greater drought sensitivity of NPP_u in younger stands (~20–35 years) could be due to an increase in: (1) competition for resources due to high understorey plant density; (2) heat stress as a result of increased exposure to incoming solar radiation and radiative soil warming; and (3) soil water depletion attributable to increased evapotranspiration. The subsequent decrease in the negative impact of drought on NPP_u in older stands may be related to the age-related decline in understorey biomass and production^{26,33}. Moreover, the capacity of overstorey to act as thermal forest-floor insulator (Extended Data Fig. 8) through shading and transpirational cooling may mitigate drought stress for the understorey³⁴. This effect may, however, be compensated by an increase in rainfall interception and tree transpiration, which consequently may lead to a reduction in soil water storage with the increase in tree biomass. In addition, the age-related changes in the drought response of NPP (and subsequently NEP) might also result from contrasting drought tolerances within the tree layer during stand development. In particular, tree age and/or size have been previously noted

as key factors in controlling the drought response of tree growth^{18–23}. Possible mechanisms causing such age- and/or size-related variations may include changes in leaf-to-sapwood area ratio³⁵ and/or greater access to soil water provided by deeper, more extensive tree rooting systems³⁶, which tend to counteract the effect of the increasing hydraulic challenge, water requirements and evaporative demand experienced by trees during stand development^{21,37}. At present, however, it remains inconclusive whether forest stands consisting of young (small) or old (large) trees are more resistant to drought, particularly in the boreal region. Although we observed that the production of trees in young stands was somewhat less resistant to drought, overall our findings do not strongly support the hypothesis of a significant age-dependent drought sensitivity of NPP_t. Nonetheless, a more detailed understanding of how trees at various growth stages respond to drought is warranted, as it may have important implications for regeneration failure and/or future forest composition and structure³⁸.

During the 2018 drought, both understorey and tree production were reduced, but in general they allocated relatively more biomass to roots than to aboveground components (Extended Data Fig. 9), likely to improve access to soil water. While this strategy for coping

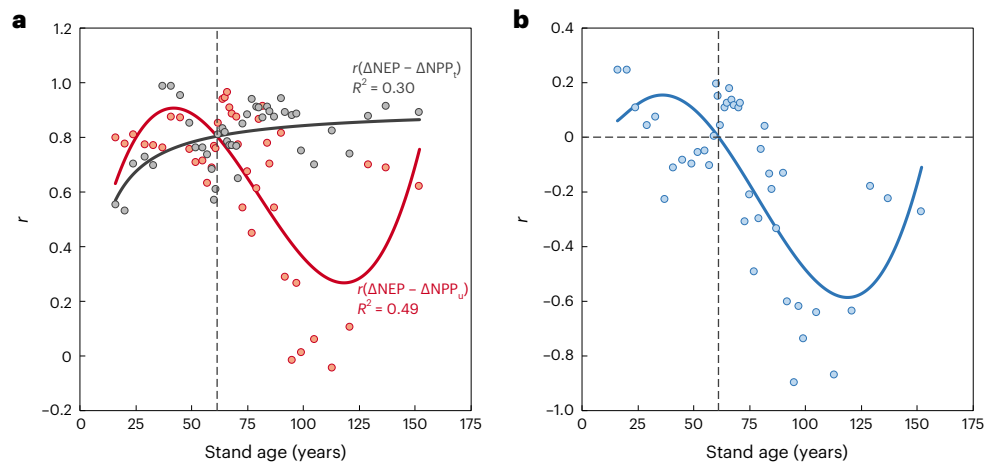


Fig. 4 | Age-related shift in understorey versus tree production regulates the drought response of forest NEP. a, Moving-window correlations between the absolute anomaly of NEP (ΔNEP) and the absolute anomalies of NPP of trees and understorey (ΔNPP_t and ΔNPP_u , respectively) over stand age. Analyses were conducted using a window of seven forest stands with a step of one forest stand. For each relationship, circular open symbols indicate the Pearson's correlation coefficient (r) values for each stand age, while solid lines show the best-fit regressions (see Supplementary Table 1 for further details). **b**, Differences

between the correlation coefficients of each relationship for each stand age (circular open symbols) and the fitted regression (solid line). On the x axis, stand age corresponds to the mean age of the seven-forest-stand window. The vertical dashed line indicates the stand age at which ΔNPP_t becomes dominant over ΔNPP_u in the response of ΔNEP , which occurs at ~61 years. The horizontal dashed line shows the negative-to-positive transition in the correlation coefficient difference.

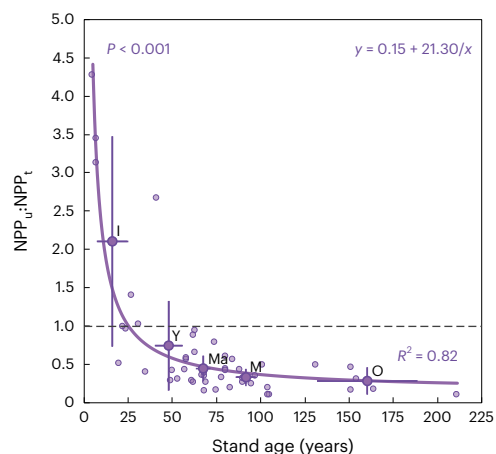


Fig. 5 | Age-related shift in the ratio of understorey to tree production. The data show the ratio of understorey to tree NPP ($NPP_u:NPP_t$) estimated for the period 2016–2018. Circular open symbols indicate the values for each forest stand, while circular filled symbols indicate the means for each of the stand age classes, including initiation (I), young (Y), middle-aged (Ma), mature (M) and old-growth (O). The horizontal and vertical bars represent the 95% confidence intervals, while the solid line shows the best-fit regression. The equation form and coefficient of determination (R^2) of the linear regression are also presented. Equation and associated goodness-of-fit statistics are derived from the individual forest stand data ($n = 49$). The P value for the non-parametric Kruskal–Wallis rank sum test comparing the differences between the means of stand age classes is also shown. The horizontal dashed line indicates the equal contribution of NPP_u and NPP_t to NPP.

with drought stress is well known³⁹, our results suggest a divergent age-related pattern. Specifically, trees and understorey prioritized belowground C allocation in the younger and older stands, respectively, which may be related to a competitive gradient with the respective dominant layer during stand development. This finding illustrates that the role of competition for resources in the root system becomes more critical under drought stress⁴⁰. This strategy could be adopted by plants to maximize survival and might be more prominent (that is, higher C root investment) in the understorey than in the trees. Our work

therefore suggests that both understorey and overstorey components in boreal forests experience greater susceptibility to drought events when facing high inter-layer competitive stress.

Our phenological observations provide further evidence that the impact of drought on the seasonal development of understorey biomass was greater than that on trees. In particular, the trees exhibited a steady decrease in greenness throughout the 2018 growing season and maintained a phenological timing consistent with normal conditions. In contrast, the short peak growing season of the understorey and its anticipated senescing stage, triggered by the summer drought, was partly due to the legacy effects of the preceding warm and sunny spring. The latter promoted an early and rapid understorey development, which was not evident in the case of trees. This fact may have contributed to earlier topsoil water depletion through enhanced water consumption and forest-floor evapotranspiration, which ultimately may have induced a greater reduction in C assimilation in understorey than in trees later in the summer. Similar to our findings, previous studies have reported the effect of earlier spring greening on vegetation growth during a drought year^{41,42}. Overall, this suggests that the peak growing season is the most sensitive phenological stage to drought, with carry-over effects from spring vegetation phenology, particularly for the understorey, strongly influencing the subsequent repercussions of summer droughts on the C sink of boreal forests.

Overall, NPP was more sensitive to drought stress than RH and acted as the primary factor contributing to the change in NEP. These observations align with previous reports across multiple biomes^{13,43,44}, suggesting that climate-driven alterations in production, rather than respiration, may emerge as key drivers in regulating the C sink strength across the boreal forest landscape. In contrast, a recent study based on a network of eddy covariance observations in 11 Nordic forests⁹ identified RH as the driver of the forest NEP anomaly across Scandinavia and the Baltic region in 2018. This divergence may indicate that RH could be more important in regulating the drought response of NEP at larger latitudinal scales compared with our studied boreal landscape. However, in contrast to our empirical assessment of NPP and RH dynamics, it should be noted that RH was not directly measured in ref. 9, but rather derived from the partitioning of ecosystem respiration, assuming autotrophic respiration as a fixed fraction of gross primary production

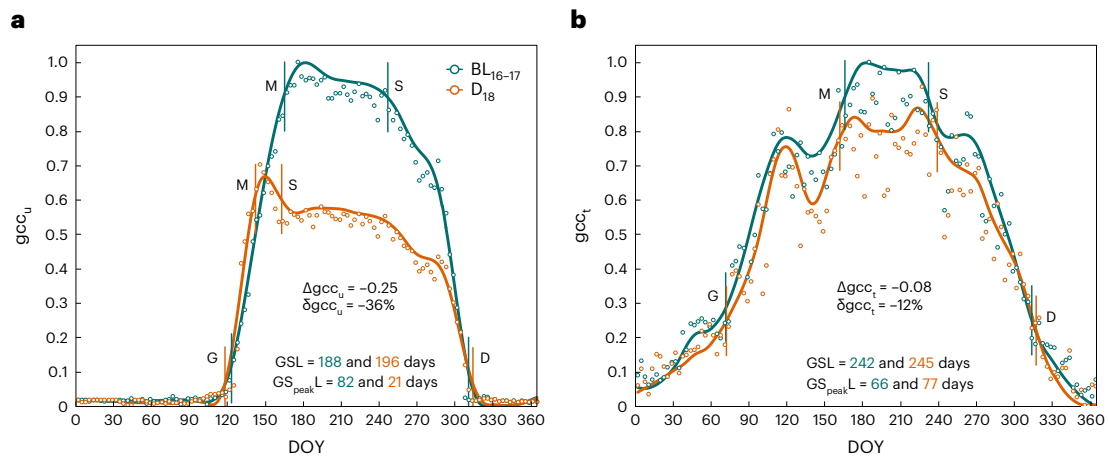


Fig. 6 | Divergent drought impact on understorey and tree phenology. **a, b**, Normalized green chromatic coordinate (gcc) for understorey (gcc_u ; **a**) and trees (gcc_t ; **b**) during the baseline period 2016–2017 (BL_{16–17}) and the drought year 2018 (D₁₈) over the day of the year (DOY). Circular open symbols and lines correspond to the 3-day means of normalized gcc and locally estimated scatterplot smoothing (loess) fits, respectively. Mean values of the absolute and

relative anomalies of gcc_u (Δgcc_u and δgcc_u , respectively) and gcc_t (Δgcc_t and δgcc_t , respectively) during the growing season are also shown. Furthermore, the transition dates between the phenological stages of green-up (G), maturity (M), senescence (S) and dormancy (D) are indicated by vertical lines. The length in days of both the total and peak growing season (GSL and GS_{peakL} , respectively) are also reported.

across all sites and environmental conditions. Nevertheless, although both approaches suffer from method-specific shortcomings, these contrasting findings emphasize the need for a better understanding of the individual component fluxes that regulate the impact of drought on the forest C balance.

Managing the boreal forest NEP in a future drier climate

Our results showed that the NEP was considerably reduced by drought (on average by 80 ± 16 g C m⁻² yr⁻¹ or $57 \pm 13\%$) across the managed landscape. It is worth noting that the NEP reduction in our mature forest stands (58 ± 31 g C m⁻² yr⁻¹) was closely related to independent eddy covariance observations conducted in forest stands of similar age class, both within and in close vicinity of the studied landscape (Methods and Supplementary Table 2; ~ 41 – 59 g C m⁻² yr⁻¹). Furthermore, this decline in the forest C sink during the 2018 drought is consistent with that estimated (87 ± 87 g C m⁻² yr⁻¹) from observations reported in the recent eddy-covariance-based study⁹. Considering the broad range (10th–90th percentile) of 8 – 154 g C m⁻² yr⁻¹ or 3 – 111% observed in the drought-induced NEP reduction across the studied forest stands, our results suggest, similarly to previous eddy-covariance-based reports^{9,13}, that the weakening of the forest C sink is highly variable across the heterogeneous landscape. This spatial variation needs to be taken into account when extrapolating the future drought response of the forest C balance across the boreal biome.

Our study further explored the importance of key spatial attributes in determining the impact of drought on forest NEP across the managed boreal landscape. It was somewhat surprising to find that soil type and dominant tree species did not have a significant impact on the drought response of NEP, despite previous studies demonstrating interaction effects between drought, soil and tree species on tree growth^{45–47}. This result may be related to the counterbalancing drought responses of the NEP components (Extended Data Figs. 3 and 7) and/or the similar development of drought impact (Supplementary Fig. 2) between sediment–till soils and pine–spruce stands. It is also worth noting that our studied forest stands were not pure monocultures²⁶. Therefore, it is possible that the mixture of tree species may have levelled out to a similar stand-level drought response^{45,48}. Our results suggest that variations in forest age structure, including understorey-tree composition, may largely outweigh the effects of soil conditions and

tree species distribution in controlling future drought impacts on the C sink strength of boreal forests.

The age-dependent drought sensitivity of NEP implies that the response of the forest C balance to more frequent and severe droughts projected for northern latitudes during the twenty-first century^{6,7} may be largely non-uniform across the boreal forest landscape. At present, approximately two-thirds of the boreal forest biome is actively managed⁴, resulting in a complex mosaic of forest stands at varying developmental stages. Consequently, large gradients in the drought response of NEP can be expected across managed landscapes, a fact that may be particularly important in Fennoscandia, where up to 90% of the forest area is managed⁴. Furthermore, these managed landscapes are dominated by a large proportion of young forest stands (Extended Data Fig. 10) and hence, according to our results, may experience a greater drought-induced NEP reduction. Thus, a shift towards young forest stands at the present⁸ or at even higher rates as a result of more frequent stand-replacing disturbances^{49,50} and/or shorter rotation periods, might critically weaken the C sink strength of the boreal landscape under future droughts. Therefore, forest management strategies that promote the transition to late-successional stands (for example, increasing the share of continuous cover forestry and/or extending the rotation period) may have the potential to increase the drought resistance of the C sink of the boreal forest landscape.

Online content

Any methods, additional references, Nature Portfolio reporting summaries, source data, extended data, supplementary information, acknowledgements, peer review information; details of author contributions and competing interests; and statements of data and code availability are available at <https://doi.org/10.1038/s41561-024-01374-9>.

References

- Bonan, G. B. & Shugart, H. H. Environmental factors and ecological processes in boreal forests. *Annu. Rev. Ecol. Syst.* **20**, 1–28 (1989).
- Pan, Y. et al. A large and persistent carbon sink in the world's forests. *Science* **333**, 988–993 (2011).
- Bradshaw, C. J. A. & Warkentin, I. G. Global estimates of boreal forest carbon stocks and flux. *Glob. Planet. Change* **128**, 24–30 (2015).

4. Gauthier, S. et al. Boreal forest health and global change. *Science* **349**, 819–822 (2015).
5. Seidl, R. et al. Forest disturbances under climate change. *Nat. Clim. Change* **7**, 395–402 (2017).
6. Dai, A. Increasing drought under global warming in observations and models. *Nat. Clim. Change* **3**, 52–58 (2013).
7. Spinoni, J. et al. Will drought events become more frequent and severe in Europe? *Int. J. Climatol.* **38**, 1718–1736 (2018).
8. McDowell, N. G. et al. Pervasive shifts in forest dynamics in a changing world. *Science* **368**, eaaz9463 (2020).
9. Lindroth, A. et al. Effects of drought and meteorological forcing on carbon and water fluxes in Nordic forests during the dry summer of 2018. *Phil. Trans. R. Soc. B* **375**, 20190516 (2020).
10. Doughty, C. E. et al. Drought impact on forest carbon dynamics and fluxes in Amazonia. *Nature* **519**, 78–82 (2015).
11. Machado-Silva, F. et al. Drought resilience debt drives NPP decline in the Amazon forest. *Glob. Biogeochem. Cycles* **35**, e2021GB007004 (2021).
12. Zhao, M. & Running, S. W. Drought-induced reduction in global terrestrial net primary production from 2000 through 2009. *Science* **329**, 940–943 (2010).
13. Ciais, P. et al. Europe-wide reduction in primary productivity caused by the heat and drought in 2003. *Nature* **437**, 529–533 (2005).
14. McDowell, N. et al. Mechanisms of plant survival and mortality during drought: why do some plants survive while others succumb to drought? *New Phytol.* **178**, 719–739 (2008).
15. McDowell, N. G. et al. Mechanisms of woody-plant mortality under rising drought, CO₂ and vapour pressure deficit. *Nat. Rev. Earth Environ.* **3**, 294–308 (2022).
16. Davidson, E. A. & Janssens, I. A. Temperature sensitivity of soil carbon decomposition and feedbacks to climate change. *Nature* **440**, 165–173 (2006).
17. Moyano, F. E., Manzoni, S. & Chenu, C. Responses of soil heterotrophic respiration to moisture availability: an exploration of processes and models. *Soil Biol. Biochem.* **59**, 72–85 (2013).
18. Au, T. F. et al. Younger trees in the upper canopy are more sensitive but also more resilient to drought. *Nat. Clim. Change* **12**, 1168–1174 (2022).
19. Giardina, F. et al. Tall Amazonian forests are less sensitive to precipitation variability. *Nat. Geosci.* **11**, 405–409 (2018).
20. Liu, L. et al. Tropical tall forests are more sensitive and vulnerable to drought than short forests. *Glob. Change Biol.* **28**, 1583–1595 (2022).
21. Bennett, A. C. et al. Larger trees suffer most during drought in forests worldwide. *Nat. Plants* **1**, 15139 (2015).
22. Bartholomew, D. C. et al. Small tropical forest trees have a greater capacity to adjust carbon metabolism to long-term drought than large canopy trees. *Plant Cell Environ.* **43**, 2380–2393 (2020).
23. Li, T. et al. The forest resistance to droughts differentiated by tree height in Central Europe. *J. Geophys. Res. Biogeosci.* **128**, e2021JG006668 (2023).
24. Phillips, R. P. et al. A belowground perspective on the drought sensitivity of forests: towards improved understanding and simulation. *For. Ecol. Manag.* **380**, 309–320 (2016).
25. Ivanov, V. Y. et al. Root niche separation can explain avoidance of seasonal drought stress and vulnerability of overstory trees to extended drought in a mature Amazonian forest. *Water Resour. Res.* **48**, W12507 (2012).
26. Peichl, M. et al. Landscape-variability of the carbon balance across managed boreal forests. *Glob. Change Biol.* **29**, 1119–1132 (2023).
27. Kljun, N. et al. Response of net ecosystem productivity of three boreal forest stands to drought. *Ecosystems* **9**, 1128–1144 (2006).
28. Welp, L. R., Randerson, J. T. & Liu, H. P. The sensitivity of carbon fluxes to spring warming and summer drought depends on plant functional type in boreal forest ecosystems. *Agric. For. Meteorol.* **147**, 172–185 (2007).
29. Xu, B. et al. Seasonal variability of forest sensitivity to heat and drought stresses: a synthesis based on carbon fluxes from North American forest ecosystems. *Glob. Change Biol.* **26**, 901–918 (2020).
30. Grant, R. F. et al. Interannual variation in net ecosystem productivity of Canadian forests as affected by regional weather patterns – a Fluxnet-Canada synthesis. *Agric. For. Meteorol.* **149**, 2022–2039 (2009).
31. Peters, W. et al. A historical, geographical and ecological perspective on the 2018 European summer drought. *Phil. Trans. R. Soc. B* **375**, 20190505 (2020).
32. Nilsson, M.-C. & Wardle, D. A. Understory vegetation as a forest ecosystem driver: evidence from the northern Swedish boreal forest. *Front. Ecol. Environ.* **3**, 421–428 (2005).
33. Martínez-García, E. et al. Overstory dynamics regulate the spatial variability in forest-floor CO₂ fluxes across a managed boreal forest landscape. *Agric. For. Meteorol.* **318**, 108916 (2022).
34. De Frenne, P. et al. Global buffering of temperatures under forest canopies. *Nat. Ecol. Evol.* **3**, 744–749 (2019).
35. McDowell, N. et al. The relationship between tree height and leaf area: sapwood area ratio. *Oecologia* **132**, 12–20 (2002).
36. Nepstad, D. C. et al. The role of deep roots in the hydrological and carbon cycles of Amazonian forests and pastures. *Nature* **372**, 666–669 (1994).
37. McDowell, N. G. & Allen, C. D. Darcy’s law predicts widespread forest mortality under climate warming. *Nat. Clim. Change* **5**, 669–672 (2015).
38. Reich, P. B. et al. Even modest climate change may lead to major transitions in boreal forests. *Nature* **608**, 540–545 (2022).
39. Eziz, A. et al. Drought effect on plant biomass allocation: a meta-analysis. *Ecol. Evol.* **7**, 11002–11010 (2017).
40. Fox, A. J. & Fort, F. Root and shoot competition lead to contrasting competitive outcomes under water stress: a systematic review and meta-analysis. *PLoS ONE* **14**, e0220674 (2019).
41. Bastos, A. et al. Direct and seasonal legacy effects of the 2018 heat wave and drought on European ecosystem productivity. *Sci. Adv.* **6**, eaba2724 (2020).
42. Lian, X. et al. Summer soil drying exacerbated by earlier spring greening of northern vegetation. *Sci. Adv.* **6**, eaax0255 (2020).
43. Schwalm, C. R. et al. Assimilation exceeds respiration sensitivity to drought: A FLUXNET synthesis. *Glob. Change Biol.* **16**, 657–670 (2010).
44. Shi, Z. et al. Differential effects of extreme drought on production and respiration: synthesis and modeling analysis. *Biogeosciences* **11**, 621–633 (2014).
45. Aldea, J. et al. Timing and duration of drought modulate tree growth response in pure and mixed stands of Scots pine and Norway spruce. *J. Ecol.* **110**, 2673–2683 (2022).
46. Lévesque, M., Walthert, L. & Weber, P. Soil nutrients influence growth response of temperate tree species to drought. *J. Ecol.* **104**, 377–387 (2016).
47. Schmied, G. et al. Nutrient regime modulates drought response patterns of three temperate tree species. *Sci. Total Environ.* **868**, 161601 (2023).
48. Pardos, M. et al. The greater resilience of mixed forests to drought mainly depends on their composition: analysis along a climate gradient across Europe. *For. Ecol. Manag.* **481**, 118687 (2021).
49. Boucher, D. et al. Current and projected cumulative impacts of fire, drought, and insects on timber volumes across Canada. *Ecol. Appl.* **28**, 1245–1259 (2018).
50. Venäläinen, A. et al. Climate change induces multiple risks to boreal forests and forestry in Finland: a literature review. *Glob. Change Biol.* **26**, 4178–4196 (2020).

Publisher's note Springer Nature remains neutral with regard to jurisdictional claims in published maps and institutional affiliations.

Open Access This article is licensed under a Creative Commons Attribution 4.0 International License, which permits use, sharing, adaptation, distribution and reproduction in any medium or format, as long as you give appropriate credit to the original author(s) and the source, provide a link to the Creative Commons license, and indicate if changes were made. The images or other third party material in this

article are included in the article's Creative Commons license, unless indicated otherwise in a credit line to the material. If material is not included in the article's Creative Commons license and your intended use is not permitted by statutory regulation or exceeds the permitted use, you will need to obtain permission directly from the copyright holder. To view a copy of this license, visit <http://creativecommons.org/licenses/by/4.0/>.

© The Author(s) 2024

Methods

Study site characteristics

This study was carried out in the 68 km² Krycklan Catchment Study (KCS), which is located in the boreal region of northern Sweden (64° 14' N, 19° 46' E), ca. 60 km west of the Baltic Sea coast (Extended Data Fig. 1; see ref. 51 for further details). The climate is cold temperate humid, with permanent snow cover persisting for ca. 167 days per year from mid-November to late April. The 30-year (1991–2020) total annual precipitation averages 638 ± 40 mm (±95% confidence interval), of which approximately 30% falls as snow. The mean annual, January and July temperatures are 2.4 ± 0.3, -8.3 ± 1.0 and 15.0 ± 0.6 °C, respectively. The terrain is gently undulating and spans elevations from 339 m above sea level (a.s.l.) in the northwest to 138 m a.s.l. at the outlet in the southeastern part of the KCS. Till soils (51% of total catchment area) dominate the higher elevations, whereas the lower elevations are characterized by sediment soils (that is, silt, sand and glaciofluvial deposits; 30%). The KCS is predominantly covered by forests (87%) consisting of Scots pine (*Pinus sylvestris* L., 63%), Norway spruce (*Picea abies* (L.) H. Karst., 26%) and deciduous trees (*Betula* spp., *Alnus incana* (L.) Moench. and *Populus tremula* L., 11%). The understorey vegetation at the forest floor is composed of ericaceous shrubs, mostly bilberry (*Vaccinium myrtillus* L.) and lingonberry (*Vaccinium vitis-idaea* L.), which grow on moss mats of *Hylocomium splendens* (Hedw.) Br. Eur. and *Pleurozium schreberi* (Brid.) Mitt⁵¹. Mires (9%), arable land (2%), built-up areas (1%) and lakes (1%) encompass the remaining catchment area. A network of small streams, both naturally formed and manmade, connect the 13 partially nested sub-catchments (ranging from an area of 0.12 to 19.13 km²) to the river network⁵¹.

Environmental conditions

Environmental measurements were available for the long-term reference period 1991–2020. Specifically, air temperature at 1.7 m above ground (Ta, °C; T107, Campbell Scientific Inc.), global radiation at 1.7 m above ground (Rg, MJ m⁻²; CM11, Kipp & Zonen) and precipitation (P, mm; ARG 100, Campbell Scientific Inc) were measured in the vicinity of the central part of the KCS at the Svartberget (SVB) reference climate station (64° 14' N, 19° 46' E, 225 m a.s.l.; Extended Data Fig. 1a). In addition, the standardized precipitation evapotranspiration index (SPEI) computed at the 3-month time scale was used to characterize the drought conditions over the KCS. This was retrieved from the 0.5° gridded dataset supplied in the Global SPEI database (SPEIbase v2.8, <https://spei.csi.ces/database.html>). The estimation of the potential evapotranspiration in this database is based on the FAO-56 Penman–Monteith method.

Selected forest stands

A subset of 50 forest stands, with ages ranging from 5 to 211 years, was selected by a stratification from the KCS plot network (350 × 350 m square grid) established in autumn 2014 and comprising 556 permanent forest inventory plots (Extended Data Fig. 1a). The age (that is, number of years after stand establishment) of each plot was determined by the basal area-weighted average age, obtained by coring 8–10 dominant trees outside each plot in 2015. Forest stands were categorized into five age classes: initiation (*n* = 8), young (*n* = 9), middle-aged (*n* = 13), mature (*n* = 14) and old-growth (*n* = 6). These age classes spanned 5–27, 31–58, 61–78, 80–105 and 131–211 years old, respectively. Moreover, each forest stand was grouped by soil type (sediment and till, *n* = 15 and 35, respectively) and dominant tree species (pine and spruce, *n* = 28 and 22, respectively). It should be noted that the forest stands were not pure monocultures, but commonly included a mixture of tree species (see ref. 26 for further details). Within each forest stand, the inventory plot (10 m radius) belonging to the KCS network was used for biometric- and chamber-based CO₂ flux measurements performed during the period 2016–2018. One forest stand was subjected to thinning operations in spring 2018 and was thus excluded from the analysis to prevent confounding effects (see Supplementary Fig. 3 for further details).

Biometric- and chamber-based annual CO₂ flux estimates

Annual above- and belowground coarse root biomass stocks of living trees (diameter at breast height (DBH, 1.3 m) ≥ 3 cm; AGB_t and BGB_{t-cr}, respectively) were calculated for each inventory plot in a subset of 47 forest stands during 2016–2018 using successive forest inventories, tree increment cores (*n* = 150 trees, 2–4 representative trees per plot) and species-specific allometric equations^{52–54}. Tree seedlings and saplings (DBH < 3 cm) were not included in the inventories and their total biomass was considered negligible. Using measurements from each inventory plot, above-mentioned allometric equations and/or volume estimates as well as species- and decay-class-specific wood densities⁵⁵, we computed the annual above- and belowground coarse root biomass stocks of standing dead trees (snags, AGB_{dw-s} and BGB_{dw-s}, respectively) and the annual total biomass stock of downed dead wood (logs, B_{dw-l}). In addition, the annual litterfall production (*L*) was also measured over the 3-year study period using 3 systematically established circular funnel-shaped litter traps (area 0.25 m²) per inventory plot, which were placed 1 m above the ground level. Plant material was collected at the beginning of the snow-free period (that is, mid-May) and at monthly intervals thereafter from August to November, oven-dried (60 °C, 48 h), sorted into fractions (foliage, branches (≤1 cm), cones and miscellaneous) and weighed. Annual AGB_t, BGB_{t-cr} and *L* in 3 recent clear-cut forest stands (5–7 years old) were further estimated based on their relationships with stand age obtained from the remaining forest stands in the initiation age class as described in ref. 26. Finally, the annual aboveground NPP of trees (ANPP_t) was computed for each of the 50 forest stands by adding the annual increment in both aboveground tree and dead wood biomass (ΔAGB_t and ΔAGB_{dw-s}, respectively) and the annual *L* (equation (1)). Annual belowground NPP of coarse roots of trees (BNPP_{t-cr}) was further computed for each forest stand as the sum of the annual increment in both belowground tree and dead wood biomass (ΔBGB_{t-cr} and ΔBGB_{dw-s}, respectively; equation (2)).

$$\text{ANPP}_t = \Delta \text{AGB}_t + \Delta \text{AGB}_{\text{dw-s}} + L \quad (1)$$

$$\text{BNPP}_{\text{t-cr}} = \Delta \text{BGB}_{\text{t-cr}} + \Delta \text{BGB}_{\text{dw-s}} \quad (2)$$

Aboveground biomass of understorey vegetation growing on the forest floor, consisting of small-sized plants such as dwarf shrubs, mosses, herbs and/or lichens, was measured for each of the 50 forest stands in June and August 2017 using 3 systematically arranged quadrats (area 0.25 m²) per inventory plot. Understorey species were mainly those described above, but their contribution varied between forest stands. All understorey plants inside each quadrat were clipped, sorted by plant functional types (PFTs; lichens, herbs, mosses and dwarf shrubs), oven-dried (60 °C, 48 h) and weighed. The biomass production of each individual PFT was then added up to calculate the annual aboveground NPP of understorey (ANPP_u) in 2017. Thus, herb production was evaluated from peak standing biomass in August, whereas the production of lichens, mosses and shrubs was determined by their respective biomass increments between June and August. Annual ANPP_u in 2016 and 2018 was computed from the annual shoot length increments (ASL, mm) of dwarf shrubs. The ASL was measured in June 2019 from the 3 closest ramets of each shrub species present at 4 m intervals along a 20-m-length transect in each inventory plot. It was assumed that the proportion between the different PFTs remained constant over the 3-year study period.

Belowground fine-root production (BNPP_{fr}) was calculated for each of the 50 forest stands using the ingrowth core method. At each inventory plot, 3 plastic mesh cores (diameter 10 cm, length 30 cm) containing a fixed volume of root-free native soil were installed in June 2017. One core per plot was removed at the end of August 2017, while the remaining two were collected at the end of September 2018. On each sampling, roots were washed free of soil over a 2 mm sieve, oven-dried (60 °C, 48 h) and weighed. Initially, we computed the daily fine-root

production (FRP, $\text{g C m}^{-2} \text{d}^{-1}$; fine-roots C content was assumed to be 50% of dry biomass) of each plot in 2017. FRP was calculated from the total root biomass at the end of August 2017 divided by number of days of incubation in the field. We then obtained the corrected FRP for each plot over the entire growing season by multiplying the daily FRP by the number of growing days ($n = 122$) between June and September 2017. Subsequently, the annual BNPP_{fr} in 2018 was derived by subtracting the FRP of September 2017 from that of September 2018. Following this, the ratio of BNPP_{fr} to aboveground NPP (ANPP , $\text{ANPP}_{\text{t}} + \text{ANPP}_{\text{u}}$) calculated in 2018 was used to compute the annual BNPP_{fr} based on ANPP in 2016 and 2017. Annual BNPP_{fr} during 2016–2018 was further partitioned into understorey (BNPP_{u}) and tree ($\text{BNPP}_{\text{t-fr}}$) components. As a first step, the annual BNPP_{u} in the 3 recent clear-cut forest stands in 2018 was calculated by multiplying the ratio of the understorey fine-root to the total fine-root biomass C stock (see ref. 33 for further details about its estimation) with annual BNPP_{fr} . From these values, we determined the average ratio of above- to belowground understorey production (that is, $\text{ANPP}_{\text{u}}/\text{BNPP}_{\text{u}}$). Assuming this ratio to be constant, we derived the annual BNPP_{u} in 2018 for the remaining 47 forest stands based on their annual ANPP_{u} . Next, a linear regression between the ratio of understorey to total fine-root production (F_{u}) and aboveground NPP of vascular plants ($\text{ANPP}_{\text{u(vp)}}$) was defined on data obtained in 2018 across the 50 forest stands. Then, F_{u} in 2016 and 2017 was estimated for each forest stand using the previous linear regression along with their annual $\text{ANPP}_{\text{u(vp)}}$ values. Annual BNPP_{u} in 2016 and 2017 was thereafter calculated by multiplying F_{u} with annual BNPP_{fr} . Finally, the annual $\text{BNPP}_{\text{t-fr}}$ during 2016–2018 was computed as the difference between BNPP_{fr} and BNPP_{u} .

Annual belowground NPP of trees (BNPP_{t}) was computed for each of the 50 forest stands as the sum of $\text{BNPP}_{\text{t-cr}}$ and $\text{BNPP}_{\text{t-fr}}$ (equation (3)). Then, the annual NPP_t was calculated for each forest stand by summing ANPP_{t} and BNPP_{t} (equation (4)), while the annual NPP_u was determined as the sum of ANPP_{u} and BNPP_{u} (equation (5)). Finally, the annual total NPP was calculated for each forest stand as the sum of NPP_t and NPP_u (equation (6)). Dry biomass of snags and logs was converted to C by using species-specific C contents for each decay class^{55,56}, while the C content was considered 50% of dry biomass for the remaining NPP components. In our approach, we assumed absent or negligible C losses due to herbivory, biogenic volatile organic compounds and root exudation.

$$\text{BNPP}_{\text{t}} = \text{BNPP}_{\text{t-cr}} + \text{BNPP}_{\text{t-fr}} \quad (3)$$

$$\text{NPP}_{\text{t}} = \text{ANPP}_{\text{t}} + \text{BNPP}_{\text{t}} \quad (4)$$

$$\text{NPP}_{\text{u}} = \text{ANPP}_{\text{u}} + \text{BNPP}_{\text{u}} \quad (5)$$

$$\text{NPP} = \text{NPP}_{\text{t}} + \text{NPP}_{\text{u}} \quad (6)$$

Heterotrophic soil respiration (RH_{s}) was measured manually every 3–4 weeks during the snow-free period (that is, early May to late October) for each of the 50 forest stands during 2016–2018. CO_2 measurements were conducted in an experimental plot (1 m^2) located a few metres outside the inventory plot, where all living vegetation was clipped and roots were trenched along the plot border. CO_2 fluxes were measured with an opaque custom-made closed steady-state chamber ($45 \times 45 \times 20 \text{ cm}$) connected to a portable infrared gas analyser. Three different infrared gas analysers (MI70, Vaisala; LGR-GGA-24EP, Los Gatos Research Inc.; GasScouterTM G4301, Picarro) were used over the 3-year study period. No significant differences in CO_2 fluxes among the 3 analysers were observed in a cross-comparison.

Annual RH_{s} was estimated by defining stand-specific Arrhenius response functions that relate RH_{s} to soil temperature for the snow-free and snow-covered periods (the latter based on measurements performed in October). These functions were then used to extrapolate RH_{s} based on continuous half-hourly soil temperature records to annual

sums. It is noteworthy that soil moisture was not included as an additional factor because we observed no significant effect of soil moisture on RH_{s} . Further details about the RH_{s} estimation are shown in ref. 33. Annual heterotrophic dead wood respiration (RH_{dw}) was derived for each forest stand by multiplying the annual above- and belowground dead wood C stocks in 2016, 2017 and 2018 with their respective decomposition rate constants (k_{dw} , yr^{-1}). We used species-specific k_{dw} rates for each component and decay class^{57,58}. Then, RH_{dw} was added to RH_{s} to obtain the annual total RH (equation (7)). It is worth noting that RH_{s} was the dominant component of RH in all forest stands, while the contribution from RH_{dw} was limited to less than 5% on average²⁶. Finally, the annual NEP was determined for each of the 50 forest stands over the 3-year study period as the difference between NPP and RH (equation (8)).

$$\text{RH} = \text{RH}_{\text{s}} + \text{RH}_{\text{dw}} \quad (7)$$

$$\text{NEP} = \text{NPP} - \text{RH} \quad (8)$$

In this study, all component CO_2 fluxes ($\text{g C m}^{-2} \text{yr}^{-1}$) were presented as positive terms, whereas positive and negative NEP refers to net C sink and source, respectively. In addition, forest-floor environment records were available for each of the 50 forest stands during 2016–2018 as described in detail in ref. 33. These records included below-canopy air temperature ($T_{\text{a,bc}}$, $^{\circ}\text{C}$), soil temperature at 10 cm depth (T_{s} , $^{\circ}\text{C}$) and soil volumetric water content at 5 cm depth (SWC, %).

Vegetation phenology

Seasonal changes in understorey and overstorey vegetation greenness phenology were assessed over the 3-year study period in the central part of the KCS using the SVB experimental forest, a ~110-year-old mixed-species forest stand (that is, spruce 64%, pine 35%, and birch 1%⁵¹). Greenness was derived from hourly images collected through digital repeat photography at the Integrated Carbon Observation System (ICOS) SVB ecosystem station (named SE-Svb in the ICOS network, $64^{\circ} 15' \text{ N}$, $19^{\circ} 46' \text{ E}$, 270 m a.s.l.; <https://www.icos-sweden.se/svartberget>; Extended Data Fig. 1a). Below- and above-tree canopy images were taken with web cameras (NetCam SC IMP, StarDot Technologies), mounted on a vertical pole and the ICOS mast at 3.8 m and 36 m above the ground level, respectively, with a downward-looking angle of 12° . Specifically, a greenness index was quantified using the gcc (dimensionless, equation (9)), which uses the average digital numbers (DN , 0–255) of the red (R_{DN}), green (G_{DN}) and blue (B_{DN}) image channels within a selected region of interest.

$$\text{gcc} = G_{\text{DN}} / (R_{\text{DN}} + G_{\text{DN}} + B_{\text{DN}}) \quad (9)$$

Three-day mean time series for understorey (gcc_{u}) and trees (gcc_{t}) were then derived for the 3-year study period. This was achieved by assigning the 90th percentile of all values within a 3-day window to the centre day of a discrete (non-overlapping) moving window as described in ref. 59. The values for gcc_{u} and gcc_{t} were then normalized (0–1) to describe the seasonal minimum and maximum of vegetation biomass development. We then fitted a locally estimated scatterplot smoothing (loess) curve using the normalized data points in order to improve the visualization. We further used the gcc to derive the four successive phases of vegetation phenology, namely green-up (G), maturity (M), senescence (S) and dormancy (D). Specifically, we determined the transition dates (that is, day of the year) for G and D by extracting the 10% and 25% thresholds of the total amplitude in gcc_{u} and gcc_{t} , respectively. Similarly, the transition dates for M and S were obtained from the 90% threshold of total amplitude in both gcc_{u} and gcc_{t} . Subsequently, we calculated the length in days of the total and peak growing season (GSL and $\text{GS}_{\text{peak,L}}$, respectively) as the difference between D–G and S–M, respectively.

Eddy covariance measurements

Eddy covariance measurements at two local sites were used to support the drought response of NEP observed by our biometric- and

chamber-based approach (see Supplementary Table 2). One site was the SVB station, whose location and surrounding forest have been described above. The other site was Rosinedalsheden (ROS; 64° 10' N, 19° 45' E, 145 m a.s.l.), a ~100-year-old naturally regenerated homogeneous pine stand, located outside the KCS about 10 km south of SVB. Annual NEP values for SVB and ROS sites during the baseline period and the year 2018 were previously reported in ref. 9.

Drought anomalies of annual CO₂ fluxes and vegetation phenology

The impact of drought on annual estimates of CO₂ fluxes and gcc index was evaluated by calculating both the absolute and relative anomalies (Δ and δ , respectively) of the drought year 2018 (D_{18}) relative to the baseline period 2016–2017 (BL_{16-17}) according to equations (10) and (11):

$$\Delta X_i = X_{iD_{18}} - X_{iBL_{16-17}} \quad (10)$$

$$\delta X_i = \frac{X_{iD_{18}} - X_{iBL_{16-17}}}{X_{iBL_{16-17}}} \times 100 \quad (11)$$

where ΔX_i and δX_i are the absolute and relative anomalies of each variable (X) expressed in absolute and relative units, respectively, $X_{iD_{18}}$ and $X_{iBL_{16-17}}$ are the variable values during D_{18} and BL_{16-17} , respectively, and subscript i refers to the studied forest stand and/or understorey–tree component layer. Positive and negative anomalies represent the increase and decrease, respectively, of each variable in 2018. Note that the absolute anomalies were used to analyse the drought response of the variables.

Statistics

Linear, polynomial and nonlinear (Levenberg–Marquardt method) regression analyses were used to explore the relationships presented in Figs. 2–5. In all cases, several types of regression were evaluated and the final model was selected based on the highest R^2 criterion. Equations and associated goodness-of-fit statistics were derived from the individual forest-stand data. Non-parametric Kruskal–Wallis rank sum tests were also performed in Figs. 2–5 to examine differences between the BL_{16-17} and D_{18} periods as well as among the initiation, young, middle-aged, mature and old-growth stand age classes. These previous statistical approaches were also used in Extended Data Figs. 2–9. A moving-window correlation was conducted between the absolute anomaly of NEP (ΔNEP) and the absolute anomalies of understorey and tree NPP (ΔNPP_u and ΔNPP_t , respectively) using a seven-forest-stand window with a one-forest-stand step to identify temporal shift of the dominant contributor to ΔNEP (Fig. 4). Furthermore, a locally estimated scatterplot smoothing (loess) fit was applied as an estimate of the seasonal trajectories for the normalized gcc_u and gcc_t (Fig. 6). All analyses were conducted using SPSS software (version 29.0; IBM corp.) and MATLAB software (MATLAB R2019b, MathWorks Inc.).

Data availability

The data that support the findings of this study are openly available in the Zenodo digital repository at <https://doi.org/10.5281/zenodo.10410676>.

References

- Laudon, H. et al. Northern landscapes in transition: evidence, approach and ways forward using the Krycklan Catchment Study. *Hydrol. Process.* **35**, e14170 (2021).
- Marklund, L. G. *Biomass Functions Pine, Spruce and Birch in Sweden* (Department of Forest Survey, Swedish Univ. Agricultural Sciences, 1988).
- Petersson, H. & Ståhl, G. Functions for below-ground biomass of *Pinus sylvestris*, *Picea abies*, *Betula pendula* and *Betula pubescens* in Sweden. *Scand. J. For. Res.* **21**, 84–93 (2006).
- Repola, J. Biomass equations for birch in Finland. *Silva Fenn.* **42**, 236 (2008).
- Sandström, F. et al. Biomass conversion factors (density and carbon concentration) by decay classes for dead wood of *Pinus sylvestris*, *Picea abies* and *Betula* spp. in boreal forests of Sweden. *For. Ecol. Manag.* **243**, 19–27 (2007).
- Mäkinen, H. et al. Predicting the decomposition of Scots pine, Norway spruce, and birch stems in Finland. *Ecol. Appl.* **16**, 1865–1879 (2006).
- Shorohova, E., Kapitsa, E. & Vanha-Majamaa, I. Decomposition of stumps 10 years after partial and complete harvesting in a southern boreal forest in Finland. *Can. J. For. Res.* **38**, 2414–2421 (2008).
- Yatskov, M., Harmon, M. E. & Krankina, O. N. A chronosequence of wood decomposition in the boreal forests of Russia. *Can. J. For. Res.* **33**, 1211–1226 (2003).
- Sonnentag, O. et al. Digital repeat photography for phenological research in forest ecosystems. *Agr. For. Meteorol.* **152**, 159–177 (2012).

Acknowledgements

This study was funded by the Swedish Research Council for Environment, Agricultural Sciences and Spatial Planning (FORMAS, grants 942–2015–49 and 2020–01446 to M.P., M.B.N., H.L., T.L. and J.E.S.F.). The authors also acknowledge support from the Kempe Foundations (grant JCK–1815 to M.P., M.B.N. and H.L.; E.M.-G. received funding from this grant). We are also grateful for additional funding from the Knut and Alice Wallenberg Foundation (grants 2015.0047 and 2018.0259 to T.L., M.P. and H.L.; E.M.-G. received funding from these grants). Financial support from the Swedish Research Council and consortium partners to both the National Research Infrastructure ICOS Sweden (grants 2015–06020 and 2019–00205) and the Swedish Infrastructure for Ecosystem Science (SITES, grant 2017–00635) is also acknowledged. We also thank the staff at the Unit for Field-Based Forest Research, SLU, for support in the field data collection.

Author contributions

M.P., M.B.N. and H.L. designed the study. M.P. provided funding acquisition, project administration and resources. T.L. contributed with additional funding. M.P., M.B.N., E.M.-G., J.E.S.F. and J.W. planned and conducted the data collection. E.M.-G. and J.W. processed the data. E.M.-G., M.P. and M.B.N. analysed and interpreted the data. E.M.-G. wrote the manuscript with contributions from all co-authors.

Funding

Open access funding provided by Swedish University of Agricultural Sciences.

Competing interests

The authors declare no competing interests.

Additional information

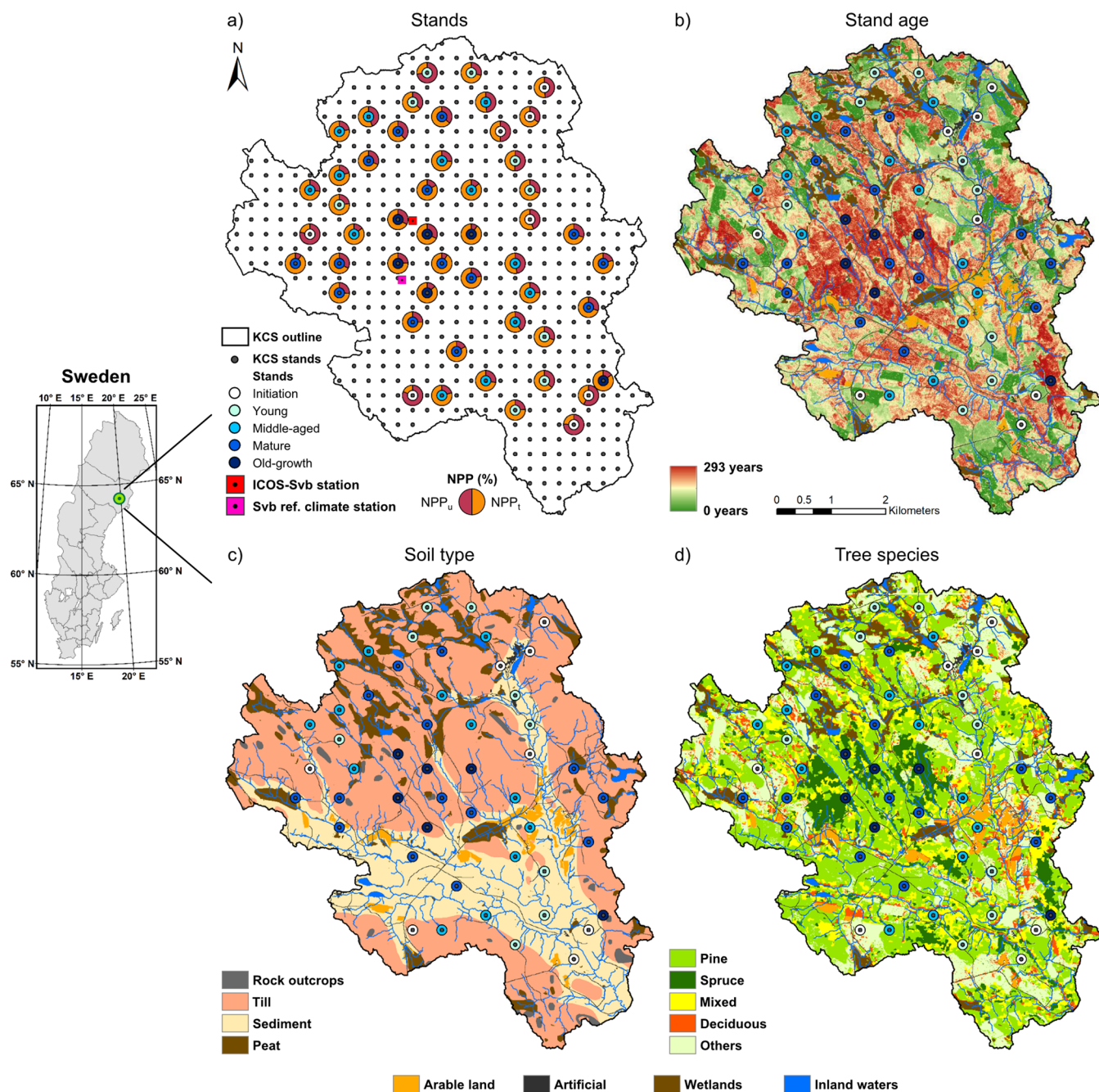
Extended data is available for this paper at <https://doi.org/10.1038/s41561-024-01374-9>.

Supplementary information The online version contains supplementary material available at <https://doi.org/10.1038/s41561-024-01374-9>.

Correspondence and requests for materials should be addressed to Eduardo Martínez-García.

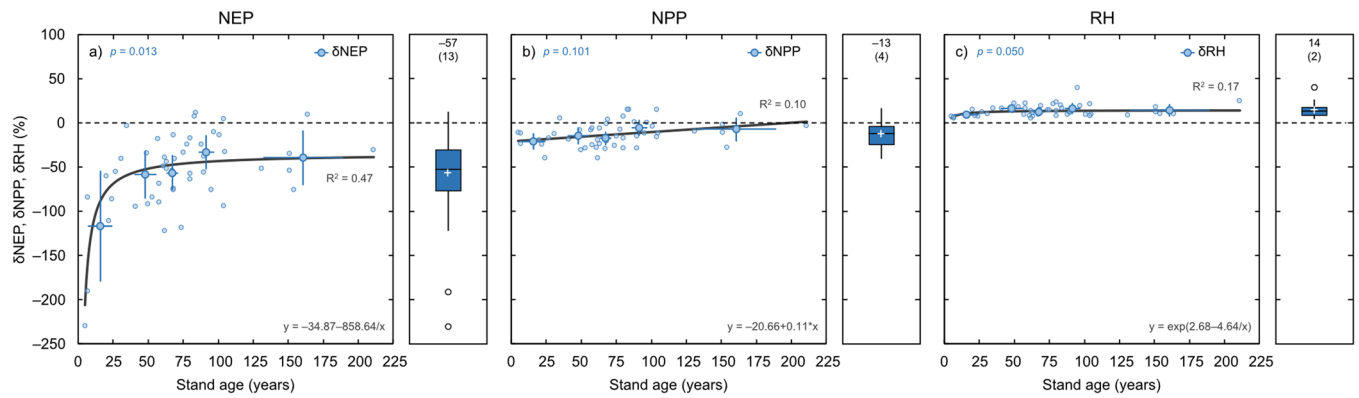
Peer review information *Nature Geoscience* thanks Michael Ryan, Tsun Fung Au and the other, anonymous, reviewer(s) for their contribution to the peer review of this work. Primary Handling Editor: Xujia Jiang, in collaboration with the *Nature Geoscience* team.

Reprints and permissions information is available at www.nature.com/reprints.



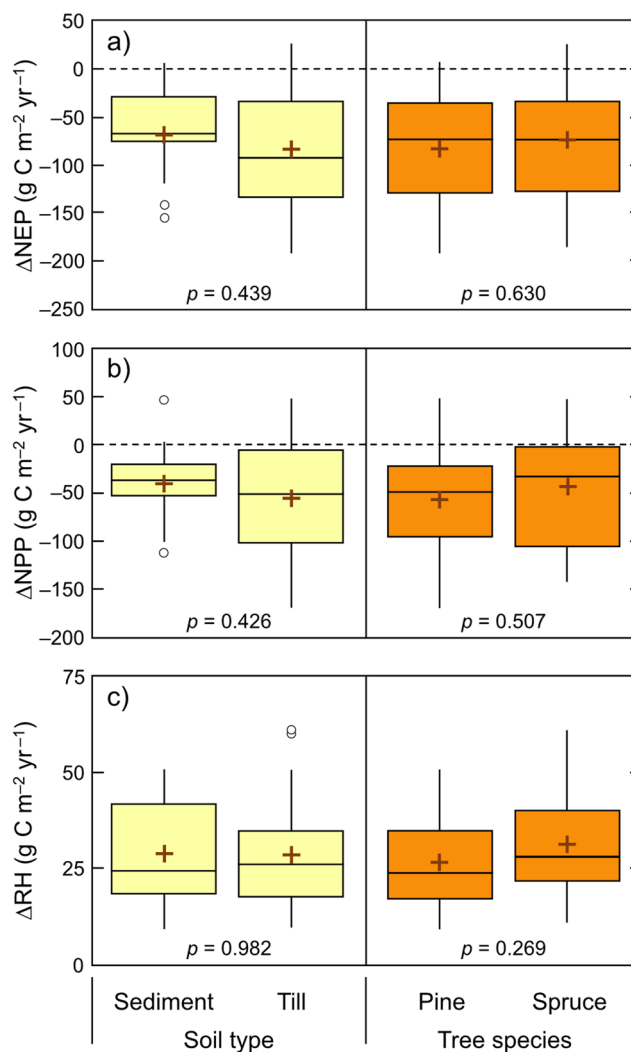
Extended Data Fig. 1 | Characterization of the Krycklan Catchment Study (KCS). The detailed map a) displays the location, stand age class, and proportion of net primary production between trees (NPP_t) and understorey (NPP_u) of the 50 selected forest stands. The map also shows the KCS' network of permanent forest inventory plots, Integrated Carbon Observation System (ICOS) Svartberget ecosystem station, and Svartberget reference climate station. The detailed map b) shows the stand age, derived from reclassifying the LiDAR-based biomass map obtained from the Swedish University of Agricultural Sciences and Swedish Forest Agency. This was achieved from the relationship between stand age (years)

and biomass (Mg ha^{-1}) defined from the 50 selected forest stands together with 50 additional forest stands ($\text{stand age} = (2.20 + 0.73 \times \sqrt{\text{biomass}})^2$, $R^2 = 0.60$, $n = 100$ forest stands). The detailed map c) illustrates the distribution of the predominant soil types (that is, Quaternary deposits; data obtained from the Swedish Geological Survey), while the detailed map d) displays the variations in the dominant tree species cover (data obtained from the Swedish Environmental Protection Agency). In addition, the detailed maps b), c), and d) show the arable land, artificial areas (that is, buildings and roads), wetlands, and inland waters (that is, lakes and streams) within the KCS.



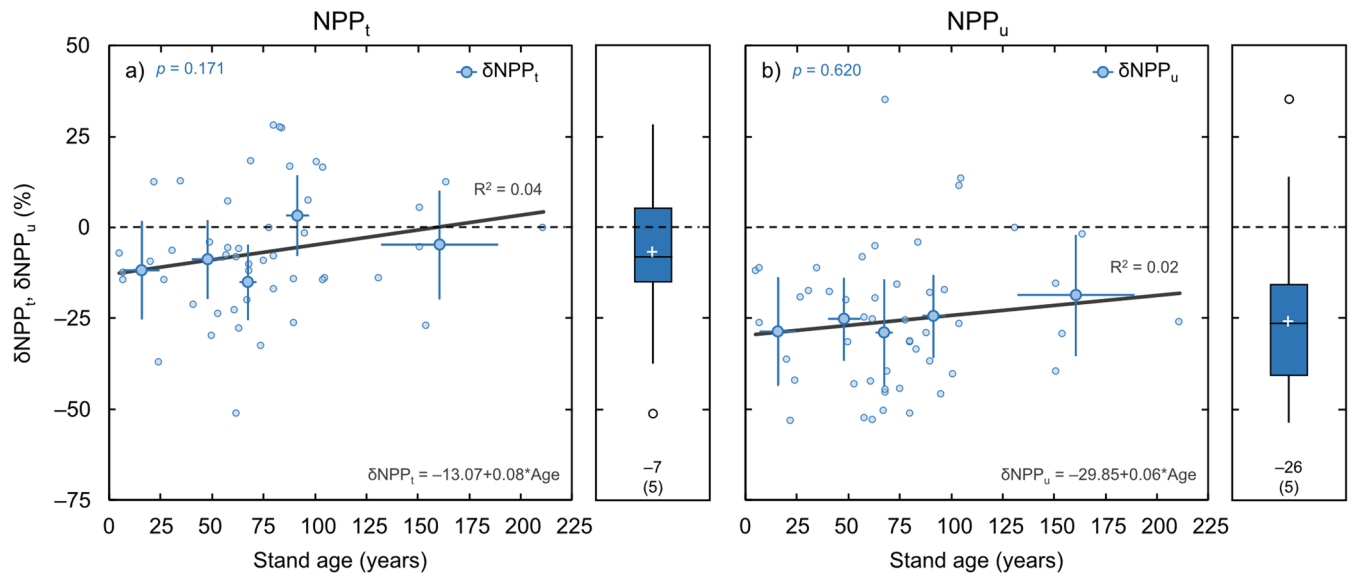
Extended Data Fig. 2 | Relative drought response of forest net ecosystem production and its component fluxes. The panels a)–c) show the relative anomalies of net ecosystem production (δNEP), net primary production (δNPP), and total heterotrophic respiration (δRH), respectively. Circular open symbols indicate the values for each forest stand, while circular closed symbols indicate the means for each of the stand age classes, including initiation (I), young (Y), middle-aged (Ma), mature (M), and old-growth (O). The horizontal and vertical bars represent the 95% confidence intervals, while the solid lines show the best-fit regressions. The equation form and coefficient of determination (R^2) of the linear regressions are also presented. Equations and associated goodness-of-fit

statistics are derived from the individual forest stand data ($n = 49$). Box plots of the relative anomalies are also shown. The boxes represent the 25th (bottom) and 75th (top) percentiles, the central line the median, and the cross the mean. Whiskers above and below the boxes denote the data within 1.5 times of the interquartile range, with outliers presented as individual points. The values show the means ($\pm 95\%$ confidence intervals) of the relative anomalies. The p -values for the non-parametric Kruskal–Wallis rank sum test comparing the differences between the means of stand age classes are also shown. The horizontal dashed lines indicate the negative-to-positive transition for the relative anomalies.



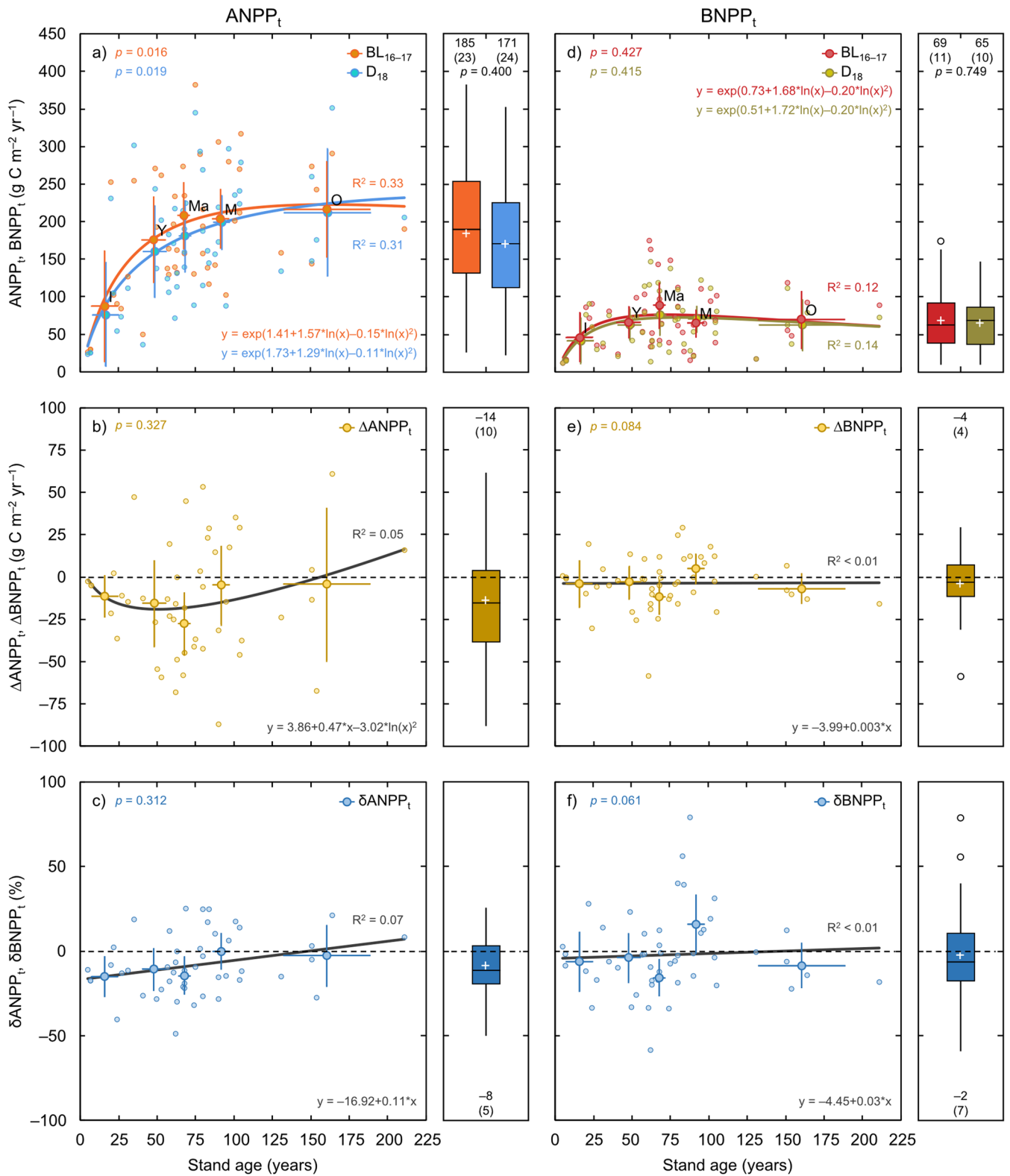
Extended Data Fig. 3 | Effect of soil type and tree species on the drought response of forest net ecosystem production and its component fluxes. The panels a)–c) show the absolute anomalies of net ecosystem production (ΔNEP), net primary production (ΔNPP), and total heterotrophic respiration (ΔRH), respectively. The boxes represent the 25th (bottom) and 75th (top) percentiles, the central line the median, and the cross the mean. Whiskers above and

below the boxes denote data within 1.5 times of the interquartile range, with outliers presented as individual points. The p -values for the non-parametric Kruskal–Wallis rank sum test comparing the differences between soil type and tree species means are also shown. The horizontal dashed line indicates the negative-to-positive transition for the absolute anomalies. $n = 49$ forest stands.



Extended Data Fig. 4 | Relative drought response of net primary production of trees and understorey. The panels a) and b) show the relative anomalies of net primary production of trees (δNPP_t) and understorey (δNPP_u), respectively. Circular open symbols indicate the values for each forest stand, while circular closed symbols indicate the means for each of the stand age classes, including initiation (I), young (Y), middle-aged (Ma), mature (M), and old-growth (O). The horizontal and vertical bars represent the 95% confidence intervals, while the solid lines show the best-fit regressions. The equation form and coefficient of determination (R^2) of the linear regressions are also presented. Equations and associated goodness-of-fit statistics are derived from the individual forest

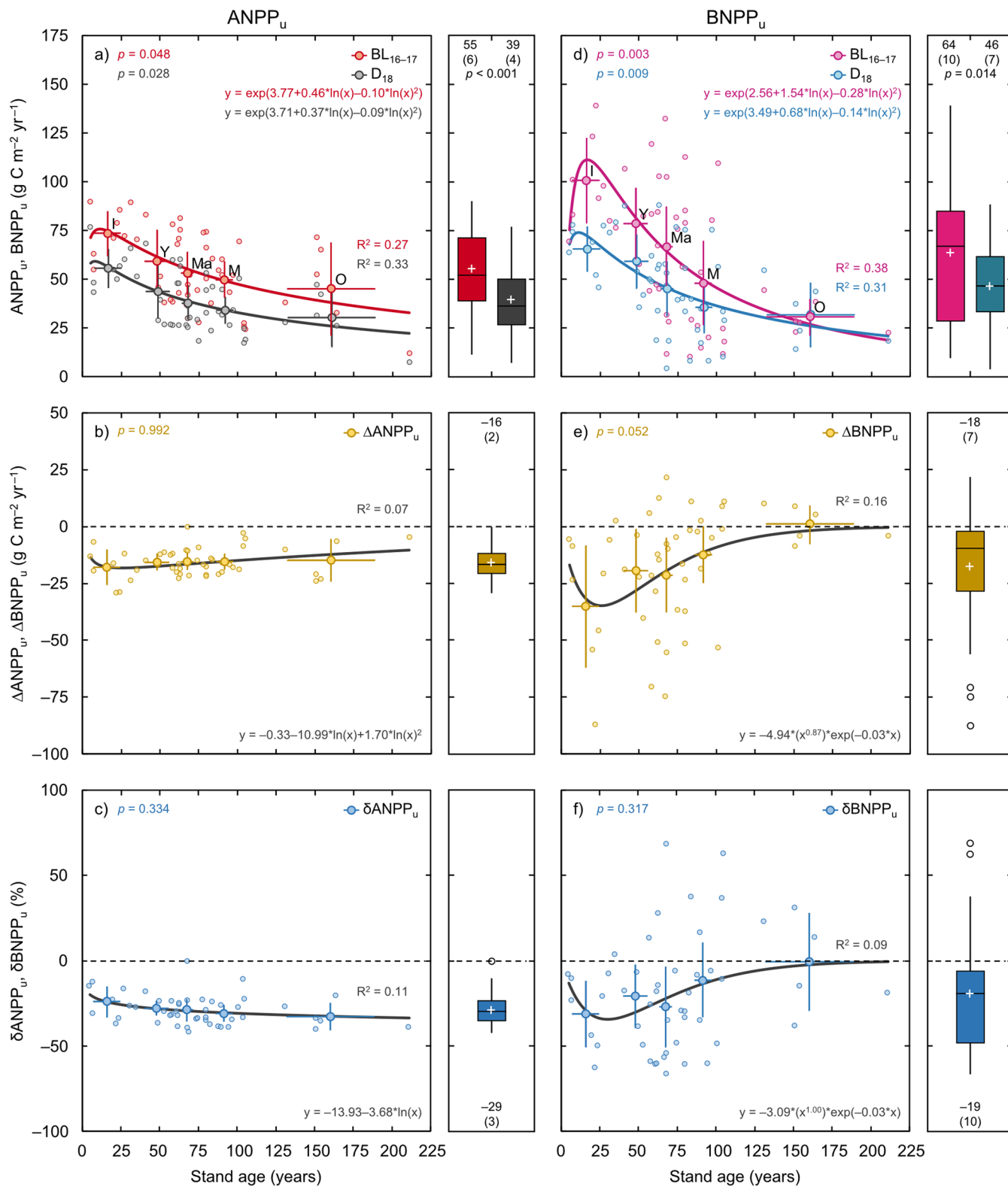
stand data ($n = 49$). Box plots of the relative anomalies are also shown. The boxes represent the 25th (bottom) and 75th (top) percentiles, the central line the median, and the cross the mean. Whiskers above and below the boxes denote the data within 1.5 times of the interquartile range, with outliers presented as individual points. The values show the means (\pm 95% confidence intervals) of the relative anomalies. The p -values for the non-parametric Kruskal–Wallis rank sum test comparing the differences between the means of stand age classes are also shown. The horizontal dashed lines indicate the negative-to-positive transition for the relative anomalies.



Extended Data Fig. 5 | See next page for caption.

Extended Data Fig. 5 | Drought response of above- and belowground net primary production of trees. The upper panels a) and d) show the annual values of above- and belowground net primary production of trees (ANPP_t and BNPP_t, respectively) for the baseline period 2016-2017 (BL₁₆₋₁₇) and the drought year 2018 (D₁₈). The middle panels b) and e) show the absolute anomalies (ΔX), while the lower panels c) and f) display the relative anomalies (δX). Circular open symbols indicate the values for each forest stand, while circular closed symbols indicate the means for each of the stand age classes, including initiation (I), young (Y), middle-aged (Ma), mature (M), and old-growth (O). The horizontal and vertical bars represent the 95% confidence intervals, while the solid lines show the best-fit regressions. The equation form and coefficient of determination (R^2) of the linear regressions are also presented. Equations and associated goodness-of-fit

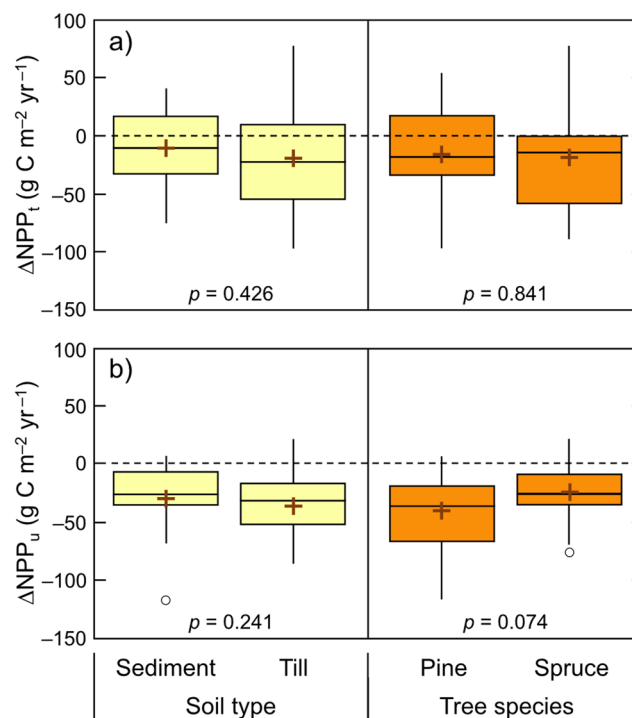
statistics are derived from the individual forest stand data ($n = 49$). Box plots of the annual values along with the absolute and relative anomalies are also shown. The boxes represent the 25th (bottom) and 75th (top) percentiles, the central line the median, and the cross the mean. Whiskers above and below the boxes denote data within 1.5 times of the interquartile range, with outliers presented as individual points. The values show the means ($\pm 95\%$ confidence intervals) of ANPP_t and BNPP_t, as well as their absolute and relative anomalies. The p -values for the non-parametric Kruskal–Wallis rank sum test comparing the differences between the means of stand age classes and BL₁₆₋₁₇–D₁₈ periods are also shown. The horizontal dashed lines indicate the negative-to-positive transition for both the absolute and relative anomalies.



Extended Data Fig. 6 | See next page for caption.

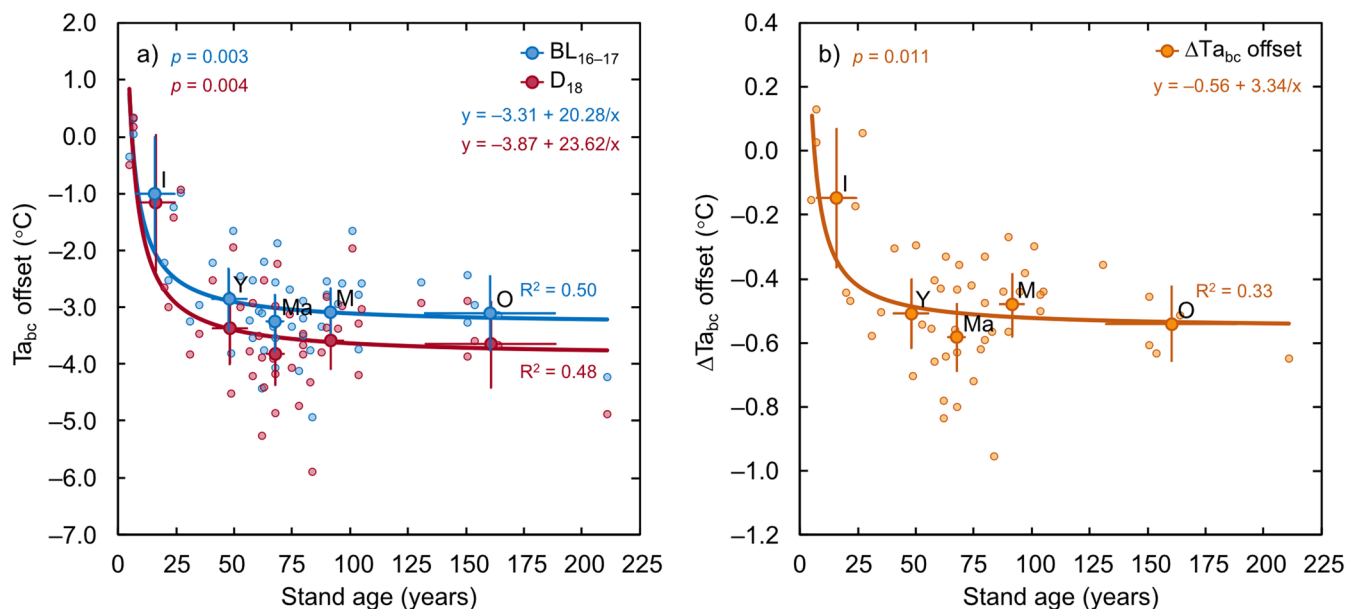
Extended Data Fig. 6 | Drought response of above- and belowground net primary production of understorey. The upper panels a) and d) show the annual values of above- and belowground net primary production of understorey (ANPP_{u} and BNPP_{u} , respectively) for the baseline period 2016–2017 (BL_{16-17}) and the drought year 2018 (D_{18}). The middle panels b) and e) show the absolute anomalies (ΔX), while the lower panels c) and f) display the relative anomalies (δX). Circular open symbols indicate the values for each forest stand, while circular closed symbols indicate the means for each of the stand age classes, including initiation (I), young (Y), middle-aged (Ma), mature (M), and old-growth (O). The horizontal and vertical bars represent the 95% confidence intervals, while the solid lines show the best-fit regressions. The equation form and coefficient of determination (R^2) of the linear regressions are also presented.

Equations and associated goodness-of-fit statistics are derived from the individual forest stand data ($n = 49$). Box plots of the annual values along with the absolute and relative anomalies are also shown. The boxes represent the 25th (bottom) and 75th (top) percentiles, the central line the median, and the cross the mean. Whiskers above and below the boxes denote data within 1.5 times of the interquartile range, with outliers presented as individual points. The values show the means (\pm 95% confidence intervals) of ANPP_{u} and BNPP_{u} , as well as their absolute and relative anomalies. The p -values for the non-parametric Kruskal–Wallis rank sum test comparing the differences between the means of stand age classes and BL_{16-17} – D_{18} periods are also shown. The horizontal dashed lines indicate the negative-to-positive transition for both the absolute and relative anomalies.



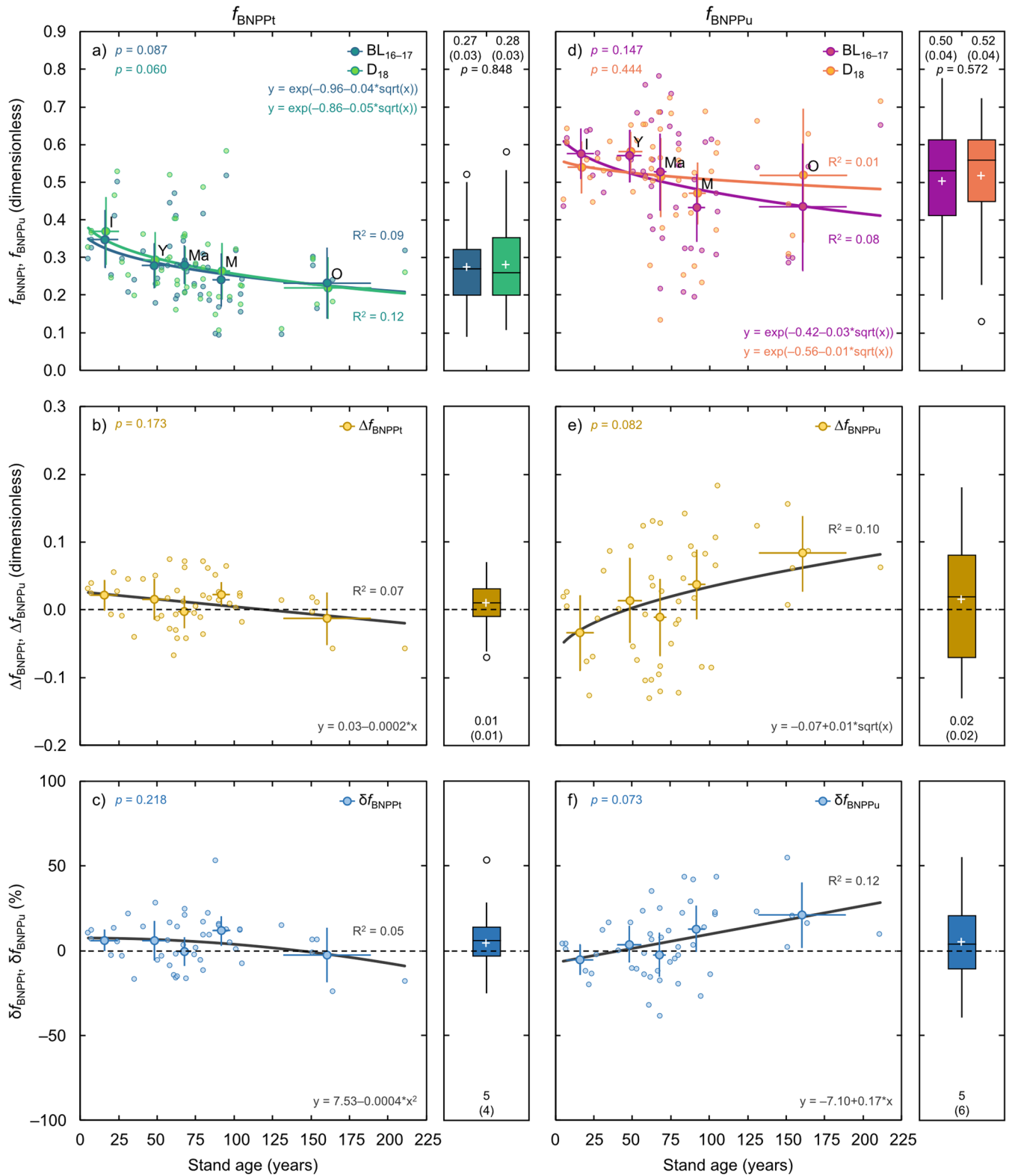
Extended Data Fig. 7 | Effect of soil type and tree species on the drought response of net primary production of trees and understorey. The panels a) and b) show the absolute anomalies of net primary production of trees (ΔNPP_t) and net primary production of understorey (ΔNPP_u), respectively. The boxes represent the 25th (bottom) and 75th (top) percentiles, the central line the median, and the cross the mean. Whiskers above and below the boxes denote data within

1.5 times of the interquartile range, with outliers presented as individual points. The p -values for the non-parametric Kruskal–Wallis rank sum test comparing the differences between the soil type and tree species means are also shown. The horizontal dashed line indicates the negative-to-positive transition for the absolute anomalies. $n = 49$ forest stands.



Extended Data Fig. 8 | Age-related shift in the air temperature offset under the forest canopy. The data show the below-canopy air temperature ($T_{a_{bc}}$) offset, which values were calculated as the difference between the mean temperature measured during May–August in each forest stand and the corresponding temperature statistic derived from the mean values recorded in the 3 youngest forest stands (5–7 years old). This latter temperature represented the air conditions outside the forest stands. Negative $T_{a_{bc}}$ offset values indicate cooler air temperatures inside than outside the forest stands. The panel a) shows the $T_{a_{bc}}$ offset during the baseline period 2016–2017 (BL₁₆₋₁₇) and the drought year 2018 (D₁₈), while the panel b) shows the absolute anomaly of $T_{a_{bc}}$ offset ($\Delta T_{a_{bc}}$)

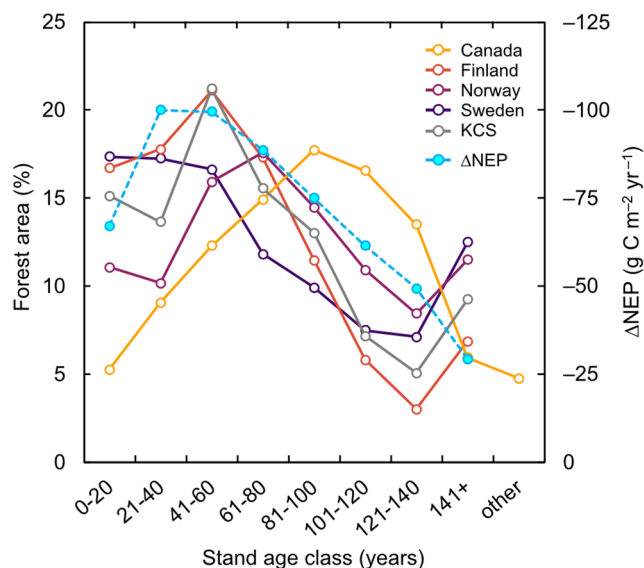
during D₁₈ relative to BL₁₆₋₁₇. Circular open symbols indicate the values for each forest stand, while circular closed symbols indicate the means for each of the stand age classes, including initiation (I), young (Y), middle-aged (Ma), mature (M), and old-growth (O). The horizontal and vertical bars represent the 95% confidence intervals, while the solid lines show the best-fit regressions. The equation form and coefficient of determination (R^2) of the linear regressions are also shown. Equations and associated goodness-of-fit statistics are derived from the individual forest stand data ($n = 49$). The p -values for the non-parametric Kruskal–Wallis rank sum test comparing the differences between the stand age class means are also shown.



Extended Data Fig. 9 | See next page for caption.

Extended Data Fig. 9 | Drought response of root biomass allocation. The upper panels a) and d) show the annual values of the fraction of the belowground to total net primary production (f_{BNPP}) for trees and understorey (f_{BNPPt} and f_{BNPPu} , respectively) for the baseline period 2016–2017 (BL_{16–17}) and the drought year 2018 (D₁₈). The middle panels b) and e) show the absolute anomalies (ΔX), while the lower panels c) and f) display the relative anomalies (δX). Circular open symbols indicate the values for each forest stand, while circular closed symbols indicate the means for each of the stand age classes, including initiation (I), young (Y), middle-aged (Ma), mature (M), and old-growth (O). The horizontal and vertical bars represent the 95% confidence intervals, while the solid lines show the best-fit regressions. The equation form and coefficient of determination (R^2) of the linear regressions are also presented. Equations and associated goodness-of-fit

statistics are derived from the individual forest stand data ($n = 49$). Box plots of the annual values along with the absolute and relative anomalies are also shown. The boxes represent the 25th (bottom) and 75th (top) percentiles, the central line the median, and the cross the mean. Whiskers above and below the boxes denote data within 1.5 times of the interquartile range, with outliers presented as individual points. The values show the means ($\pm 95\%$ confidence intervals) of f_{BNPPt} and f_{BNPPu} , as well as their absolute and relative anomalies. The p -values for the non-parametric Kruskal–Wallis rank sum test comparing the differences between the means of stand age classes and BL_{16–17}–D₁₈ periods are also shown. The horizontal dashed lines indicate the negative-to-positive transition for both the absolute and relative anomalies.



Extended Data Fig. 10 | Comparison of the age distribution of forest stands in Canada, Finland, Norway, and Sweden with the observed drought response of forest net ecosystem production. Lines represent the proportions of stand age classes (%) relative to the total forest area (that is, productive and unproductive forest). Data are based on the proportion of total forest area in: i) the boreal zone in Canada, ii) the whole country in Finland, Norway, and Sweden, and iii) 476 permanent forest inventory plots belonging to the network of the Krycklan Catchment Study (KCS). For Canada, the stand age class “other” includes forest stands with missing or unknown age class. Note that the total forest area in Finland, Norway, and Sweden is not strictly boreal⁴. Sources: Canada’s National Forest Inventory, 2007-2017 data (<http://nfi.nfis.org>), Finland’s

National Forest Inventory, 2016-2020 data (<https://statdb.luke.fi/PXWeb/pxweb/en/LUKE/>), Norway’s National Forest Inventory 2014-2018 data (<https://landsskog.nibio.no/>), and Sweden’s National Forest Inventory, 2016-2020 data (<https://skogsstatistik.slu.se/pxweb/en/OffStat/>). The absolute anomaly of net ecosystem production (ΔNEP) for each 20-year age class was also calculated from the results obtained from the forest stands studied within the KCS. For this purpose, the ΔNEP values were first calculated for each individual age (that is, 1, 2, ..., 211) and then averaged for each age class using the equation $\Delta\text{NEP} = -20.18 \times (\text{Age}^{0.62}) \times \exp(-0.016 \times \text{Age})$, $R^2 = 0.12$, shown in Fig. 2a in the main text. Negative values in ΔNEP represent a decrease in NEP during the drought year 2018.